Remote Sensing of Environment 315 (2024) 114393

Contents lists available at ScienceDirect

Remote Sensing of Environment

journal homepage: www.elsevier.com/locate/rse

Improving estimation of diurnal land surface temperatures by integrating weather modeling with satellite observations

Wei Chen [a,b], Yuyu Zhou [a,c,*], Ulrike Passe [d], Tao Zhang [j], Chenghao Wang [e,f], Ghassem R. Asrar [g], Qi Li [h], Huidong Li [i]

[a] Department of Geography, The University of Hong Kong, Hong Kong SAR 999077, China
[b] Department of Geological and Atmospheric Sciences, Iowa State University, Ames, IA 50011, USA
[c] Institute for Climate and Carbon Neutrality, The University of Hong Kong, Hong Kong SAR 999077, China
[d] College of Design, Iowa State University, Ames, IA 50011, USA
[e] School of Meteorology, University of Oklahoma, Norman, OK 73072, United States of America
[f] Department of Geography and Environmental Sustainability, University of Oklahoma, Norman, OK 73019, United States of America
[g] iCREST Foundation 3001 Bridgeway, Suite 312 Sausalito, CA 94965
[h] School of Civil & Environmental Engineering, Cornell University, Ithaca, NY 14853, USA
[i] Institute of Applied Ecology, Chinese Academy of Sciences, 110016 Shenyang, China
[j] School of Resources and Enviornment, University of Electronic Science and Technology of China, Chengdu, 611731 China

ARTICLE INFO

Edited by Jing M. Chen

Keywords:
Land surface temperature
Diurnal cycle
WRF
Morphing technique
Cloud contamination
Urban heat island

ABSTRACT

Land surface temperature (LST) derived from satellite observations and weather modeling has been widely used for investigating Earth surface-atmosphere energy exchange and radiation budget. However, satellite-derived LST has a trade-off between spatial and temporal resolutions and missing observations caused by clouds, while there are limitations such as potential bias and expensive computation in model calibration and simulation for weather modeling. To mitigate those limitations, we proposed a WRFM framework to estimate LST at a spatial resolution of 1 km and temporal resolution of an hour by integrating the Weather Research and Forecasting (WRF) model and MODIS satellite data using the morphing technique. We tested the framework in eight counties, Iowa, USA, including urban and rural areas, to generate hourly LSTs from June 1st to August 31st, 2019, at a 1 km resolution. Upon evaluation with in-situ LST measurements, our WRFM framework has demonstrated its ability to capture hourly LSTs under both clear and cloudy conditions, with a root mean square error (RMSE) of 2.63 K and 3.75 K, respectively. Additionally, the assessment with satellite LST observations has shown that the WRFM framework can effectively reduce the bias magnitude in LST from the WRF simulation, resulting in a reduction of the average RMSE over the study area from 4.34 K (daytime) and 4.12 K (nighttime) to 2.89 K (daytime) and 2.75 K (nighttime), respectively, while still capturing the hourly patterns of LST. Overall, the WRFM is effective in integrating the complementary advantages of satellite observations and weather modeling and can generate LSTs with high spatiotemporal resolutions in areas with complex landscapes (e.g., urban).

1. Introduction

Land surface temperature (LST), the radiative skin temperature of the land surface (Jaber and Abu-Allaban, 2020), provides direct insights for better understanding of Earth surface-atmosphere energy exchange and radiation budget (Li et al., 2013). The ongoing urbanization process increases LST in urban environment and significantly intensifies urban heat island (UHI) effect (i.e., elevated temperature patterns in the urban areas) (Li et al., 2022; Li et al., 2021; Li et al., 2017; Zhou et al., 2018). The diurnal LST constitutes an important element of the climate system and is vital for providing an additional constraint on latent and sensible heat flux calculations (Aires et al., 2004), detecting soil freeze/thaw status (Jiménez et al., 2015), and monitoring surface UHI (Weng and Fu, 2014).

Currently, satellite observations (Hu et al., 2022; Li et al., 2018d; Li et al., 2013; Liu et al., 2020) and physically-based weather modeling (Fu

* Corresponding author at: Institute for Climate and Carbon Neutrality & Department of Geography, The University of Hong Kong, Hong Kong SAR 999077, China
E-mail address: yuyuzhou@hku.hk (Y. Zhou).

https://doi.org/10.1016/j.rse.2024.114393
Received 4 March 2024; Received in revised form 28 July 2024; Accepted 25 August 2024
Available online 7 September 2024

et al., 2019; Li et al., 2019) offer means to understand temporal dynamics of LST and UHI effects. However, both approaches have their own limitations. Satellite observations offer an effective way to measure the spatiotemporal dynamics of LST over large areas with an acceptable accuracy, but it is limited because of the trade-off between spatial and temporal resolutions (Hu et al., 2020) and missing observations due to clouds. For example, thermal sensors on geostationary satellites, such as Spinning Enhanced Visible and InfraRed Imager (SEVIRI) and those on the NOAA Geostationary Operational Environmental Satellite (GOES), can provide LST observations in the sub-hourly frequency but with a coarse spatial resolution (i.e., several kilometers). The thermal sensors on polar-orbiting satellites, such as Moderate Resolution Imaging Spectroradiometer (MODIS), can provide global LST observations with a medium spatial resolution (i.e., 1 km) but only four observations by two different satellites (i.e., Terr and Aqua) each day. Physically-based weather modeling can provide contiguously estimates of the spatiotemporal dynamics of LST in a sub-hourly frequency and from tens of meters to thousands of kilometers in both clear-sky and cloudy conditions (Chen et al., 2011) but some potential bias still exist in the simulated LSTs due to inherent model formulations and assumptions (Liu et al., 2017; Xia et al., 2017), especially in specific seasons such as summer (Ma et al., 2015).

There have been major efforts to overcome limitations of satellite observations. These efforts fall into three categories: spatial downscaling using auxiliary data, temporal interpolation using diurnal temperature cycle (DTC) models, and fusing data from geostationary and polar-orbiting sensors. For example, auxiliary data with physical or ecological characteristics that are closely related to LST (e.g., elevation and emissivity) have been widely used to increase the spatial resolution of LST from SEVIRI and GOES to 1 km (Weng and Fu, 2014; Zakšek and Oštir, 2012). The DTC model, using quasi-physical methods with parameters ranging from two to twelve parameters (Huang et al., 2014) and semi-empirical models with more than four parameters (Göttsche and Olesen, 2001), have been widely used to describe diurnal dynamics of satellite-based LST observations and to increase their temporal resolutions (e.g., daily to hourly) (Duan et al., 2014). Both methods using auxiliary data and DTC models are helpful for the estimation of LST, but their performance was significantly influenced by the number of parameters used in these studies (Hong et al., 2018; Huang et al., 2014; Lu and Zhou, 2021). Spatiotemporal integrated temperature fusion model (STITFM) has been used to fuse multi-scale polar-orbiting and geostationary satellite observations to estimate LSTs at higher temporal and spatial resolutions, but it required similar sensor characteristics and observing conditions among multi-sensors on different satellites, such as the quality of input data, overpass times, and viewing geometry (Wu et al., 2015).

The physically-based weather modeling has also been used to estimate high spatiotemporal LSTs. The widely used Weather Research and Forecasting (WRF) model, an atmospheric modeling system designed for numerical weather prediction (Skamarock et al., 2019), couples physical parameterization schemes and satellite-observed land surface properties to simulate LST (Kirthiga and Patel, 2018). Inspired by the WRF model's sufficient physical mechanism (Chen et al., 2011), several studies have been conducted to generate MODIS-like gap-free LSTs by integrating simulated LSTs obtained from the WRF model (Fu et al., 2019; Zhang et al., 2022b; Zhang et al., 2022a; Zhang et al., 2024). In these studies, machine learning algorithms and time-adjacent strategies have been utilized to establish the relationship between MODIS-observed and WRF-simulated LSTs for reconstructing missing LST observations due to cloud contamination. However, the resulting LSTs are typically only available for the same four time points as the MODIS products. Moreover, the uncertainties present in WRF simulations may be transferred to the resulting MODIS-like LSTs. For example, one of the major sources of WRF model bias is the improper representation of land surface properties (Kirthiga and Patel, 2018). The coarse resolution and outdated satellite observations in the WRF model might fail to capture fine-scale and recent heterogeneities of land surface properties, especially in the urban domain. There is a growing body of literature on using fine resolution and updated satellite observations on land use land cover (LULC), land surface elevation, leaf area index (LAI), green vegetation fraction (GVF), and albedo to improve the accuracy of the WRF simulation (He et al., 2017; Vahmani and Ban-Weiss, 2016). Approaches such as model calibration, a procedure in which model parameters are adjusted to improve model simulations and to decrease bias in simulated LSTs compared to respective observations, can be performed using cloud computing resources (Di et al., 2018; Ji et al., 2018). However, such procedure requires tremendous computational power and professional knowledge because the WRF model involves tens to hundreds of parameters used in the model equations and they require very significant computation time to evaluate their impact on simulated LSTs.

Therefore, it is highly desirable to develop an effective method to generate accurate LSTs with high temporal and spatial resolutions devoid of the limitation's biases in observed and simulated ones. For example, MODIS observations can provide an accurate spatial pattern of LST, but the frequency of these observations are limited for a given day (i.e., four observations per day by two satellites) as well as missing observations due to cloud contamination. The WRF model has the ability to estimate diurnal LSTs, but the spatial pattern and magnitude of estimated LSTs might be biased. In this study, we propose a framework named WRFM to combine MODIS-observed and the WRF simulated LSTs to generate LSTs with high temporal and spatial resolutions. The framework benefits from integrating the diurnal pattern of LST from the WRF simulation with 1 km gap-filled MODIS LSTs (2 AM and 2 PM) (Li et al., 2018b; Pham et al., 2019; Shiff et al., 2021) to estimate the hourly LSTs at a 1 km spatial resolution. We (1) performed the WRF simulation with updated land surface properties and assessed its performance; (2) developed WRFM to integrate gap-filled MODIS LSTs and WRF simulated LSTs using morphing technique; and (3) analyzed the spatiotemporal pattern of WRFM-generated LSTs. The following sections describe the study area and data (Section 2), the proposed framework (Section 3), the results (Section 4), discussion (Section 5), and conclusions (Section 6).

2. Study area and data

2.1. Study area

The study area covers eight counties located in the central part of Iowa, USA, including Guthrie, Dallas, Polk, Jasper, Adair, Madison, Warren, and Marion counties. Polk County is not only the most populous county in Iowa (United States Census Bureau, 2020) with approximately 490 thousand inhabitants in 2019 (Li et al., 2018c), but also the home to the state capital, Des Moines. Warren, Jasper, and Dallas Counties have a mix of urban and rural areas and Dallas County is a rapidly growing county. Guthrie, Adair, Madison, and Marion Counties are mostly covered by rural areas and the Marion County is the home to Lake Red Rock, Iowa's largest lake. Three nested domains (Fig. 1A) of the WRF model were designed to cover the entire study area. The horizontal grid spacing of these three domains is 9 km (d01), 3 km (d02), and 1 km (d03), with 70×61, 126×99, and 177×102 grid cells, respectively. To further validate the performance of WRF and WRFM with in-situ measured LSTs, another two nested domains (Fig. 1B) of the WRF model were designed within d01 to cover the nearest Surface Radiation Budget Network (SURFRAD) station, Sioux Falls, South Dakota, USA (SXF). The horizontal grid spacing of these two domains is 3 km (d01s), and 1 km (d02s), with 30×30 and 30×30 grid points, respectively.

2.2. LST data

We obtained in situ near-surface air-temperature data from the NOAA-ASOS network (Automated Surface Observing System) and in situ LST measurements from the SURFRAD. NOAA-ASOS measurements are

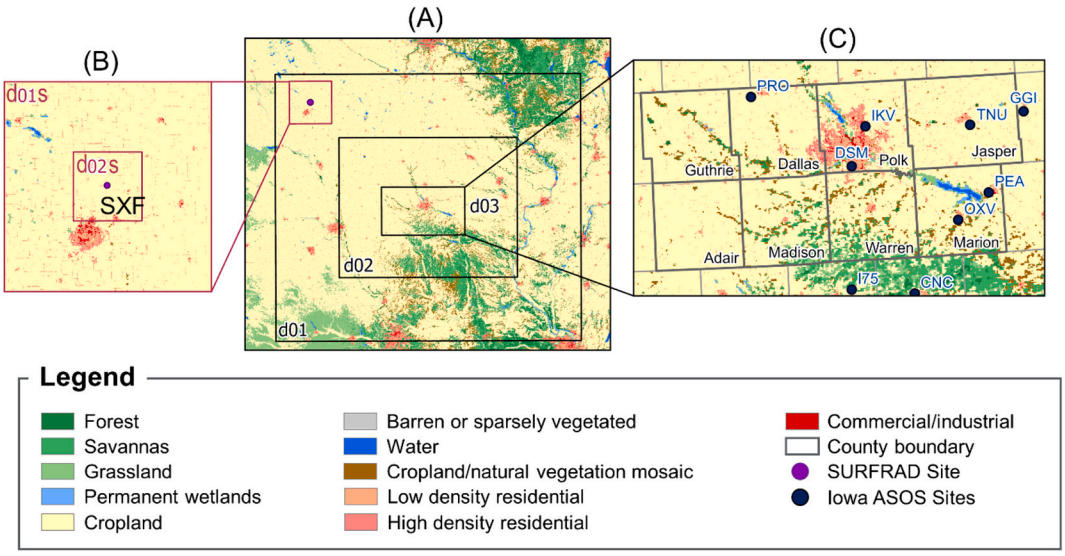

Fig. 1. The nested domains used in the WRF model for simulating LSTs in the study area (A) and SXF SURFRAD station (B). The simulation results for the innermost domain (C) were used to generate WRFM-LSTs for the study area. The background shows land cover types.

taken primarily with heated tipping bucket gages located at airports, consisting of hourly weather observations for several weather variables, including 2 m air temperature (Fullhart et al., 2020). We extracted air temperature records from June 1 to August 31, 2019 from nine ASOS stations located in the study area to assess the performance of WRF model. Furthermore, SURFRAD surface radiation budget network, consisting of seven sites across the US, was established to support satellite retrieval validation, modeling, and climate, hydrology, and weather research (Augustine et al., 2000). Using the process described in (Zhu et al., 2022) and (Duan et al., 2012), we calculated hourly in situ LSTs based on observed downwelling and upwelling longwave radiations. The accuracy of in situ LST measurements is approximately 0.5–0.8 K (Wang and Liang, 2009).

Original MODIS LSTs from June 1st to August 31st, 2019, were used to assess the spatial pattern captured by WRF-simulated and WRFM-generated LSTs. The MODIS product (MOD/MYD11A1) provides daily 1 km LSTs with four observations at ~1:30 AM and PM local time (Aqua satellite) and at ~10:30 AM and PM local time (Terra satellite). The LSTs product were derived using the refined generalize split-window LST algorithm (Wan and Dozier, 1996) with an error of about 2 K for all test

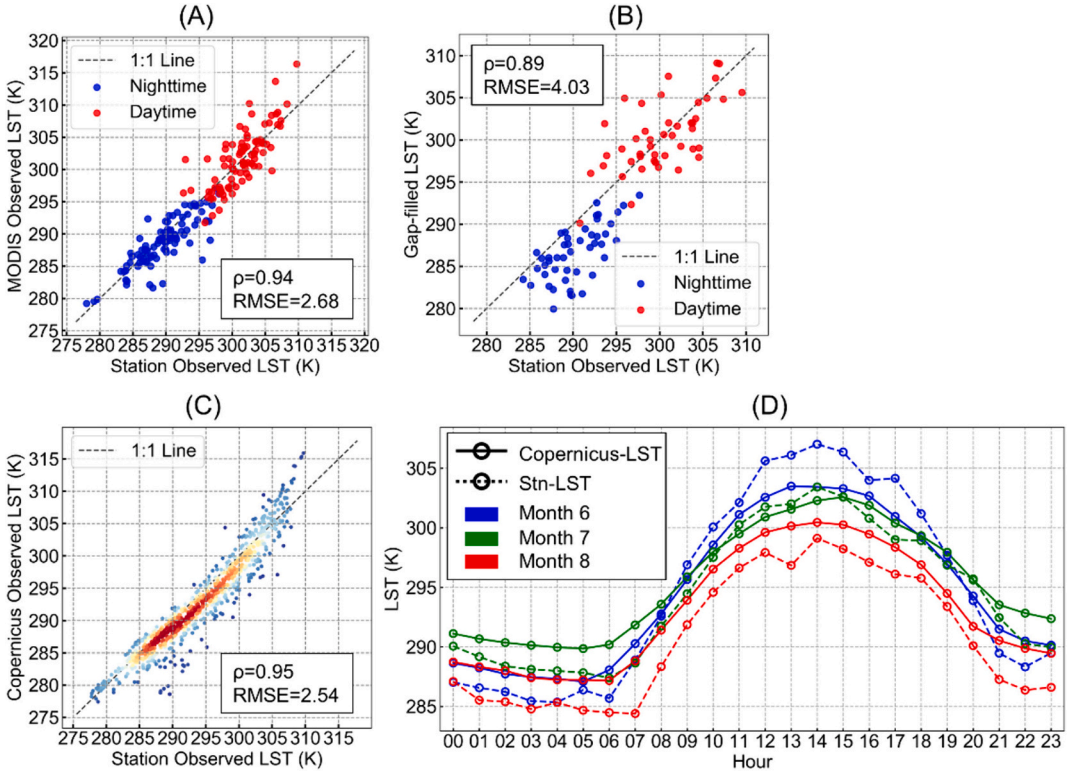

Fig. 2. The scatter plots between SURFRAD-observed and MODIS-observed (A, clear-sky), Gap-filled (B, cloudy sky), and Copernicus-observed (C, clear-sky) LSTs. The averaged diurnal variations for LSTs from SURFRAD (Stn-LST) and Copernicus (Copernicus-LST) observations in June, July, and August, respectively (D).

sites (Wan, 2014). Cloud-contaminated pixels were replaced with missing values based on the MODIS product's quality assurance (QA) information.

Gap-filled clear-sky 1 km daily LSTs from June 1st to August 31st, 2019, created by (Zhang et al., 2022c), were used to integrate with WRF-simulated LSTs. To achieve seamless daily LST coverage at mid-daytime (1:30 PM) and mid-nighttime (1:30 AM), a spatiotemporal fitting approach was employed to estimate LST values for the missing MODIS Aqua observations at 1:30 PM and 1:30 AM. This estimation was based on two other LST observations from the Terra satellite, specially at 10:30 AM and 10:30 PM. The performance of proposed framework was evaluated by calculating root mean square error (RMSE) for 15 MODIS tiles in 2005, 2010, and 2015 with introduced gaps under three scenarios (i.e., excluding 25 %, 50 %, and 75 % of valid pixels). For different ratios of exclusions, the RMSE varied from 2.05 to 2.31 °C for daytime and from 1.35 to 1.62 °C for nighttime, respectively. This LST dataset has a notable advantage in its ability to accurately capture intricate details of spatial heterogeneity within urban regions (Zhang et al., 2022c). As illustrated in Fig. 2 A&B, the estimated LSTs for the SXF SURFRAD station, derived from the gap-filled LSTs product, exhibit a competitive performance when compared with MODIS LST observations. Remarkably, the gap-filled LSTs product only shows a slight increase in RMSE of 1.35 K, highlighting its potential as a reliable data source for supplying LSTs in cases when original MODIS LSTs have missing values due to cloud contamination.

The LST data from European Copernicus satellite for June 1st to August 31st, 2019, were obtained and used to assess the diurnal variation of LST from the WRF simulation and the WRFM framework. The Copernicus Global Land Service (Freitas et al., 2013) provides hourly LSTs with a spatial resolution of 5 km for the globe's land surface within the −60°/70° latitude range. The LSTs in this product were estimated from Top-of-Atmosphere brightness temperatures from the infrared spectral channels of a constellation of geostationary satellites including Meteosat Second Generation (MSG), GOES, and Multifunction Transport Satellite (MTSAT). As a Level 4 LST product, the Copernicus LST product is considered reliable, with an uncertainty range of 2 °C (for Generalized Split-Window and the two-channel algorithm) to 4 °C (for the one-channel algorithm) (Jia et al., 2023). For our study area, the RMSE of Copernicus LSTs was 2.54 K and the Pearson's correlation coefficient (ρ) was 0.95 when compared to in situ LST measurements (Fig. 2C). While Copernicus observations can effectively capture the diurnal variation of LSTs, but they exhibit a noticeable bias in their magnitude (Fig. 2D). Therefore, Copernicus observed LST with a resolution of 5 km is suitable for validating temporal patterns.

2.3. Land surface properties for WRF modeling

We collected satellite-based land surface properties (i.e., LULC, impervious surface area (ISA), albedo, GVF, and LAI) for the study period. Usually, the WRF model uses default satellite-based land surface properties, with a coarse spatial resolution, which might be outdated and do not capture the changes and seasonal dynamic of these properties. An accurate representation of the land surface is important to precisely capture their LST effects using the WRF model (Sertel et al., 2010).

A growing body of literature shows that default land surface properties, such as LULC, ISA, albedo, GVF, and LAI, could induce significant model bias (Meng et al., 2018). First, an up-to-date LULC dataset of high spatial resolution is desirable in the WRF simulations because the WRF model uses LULC classes to assign certain static parameters and initial values at each grid cell, such as surface roughness and emissivity (Schicker et al., 2016). Second, vegetation conditions should be updated as a function of time in the WRF model using monthly gridded remote sensed GVF and LAI datasets. GVF, acting as the weighing factor between bare soil and canopy transpiration, affects LST simulation by altering surface fluxes (Chen et al., 1996). LAI plays a major role in determining the amount of transpiration from the vegetation canopy, affecting LST simulation through the alteration of evaporative cooling (Kurkowski et al., 2003). Third, physical characteristics of land surface altered by urbanization (Vahmani and Ban-Weiss, 2016; Vahmani and Hogue, 2014) should be updated in an accurate and timely manner in the WRF model using gridded monthly remotely sensed albedo and annual ISA.

All data collection and analysis for updating the land surface properties were performed on the Google Earth Engine (GEE) platform using its archived satellite observations. In accordance with previous studies (Fu and Weng, 2018; Jiang et al., 2008), LULC satellite observations were extracted from MODIS land cover (MCD12Q1.006) for the year 2019, coupled with detailed urban land use data derived from the National Land Cover Database (NLCD) for the same period (Chen et al., 2004). Given the global availability of MODIS land cover data spanning from 2001 to 2021 and the possibility of obtaining detailed urban land use data from alternative sources (Chen et al., 2014; He et al., 2019), the utilized land cover scheme in this study is adaptable for use in other study areas. The GVF values were calculated using the equation in (Gutman and Ignatov, 1998) with the MODIS (MOD13A1.006) Normalized Difference Vegetation Index (NDVI) dataset for summer of 2019 and the MODIS land cover (MCD12Q1.006) dataset for 2019. The surface albedo was calculated using the equation in (Li et al., 2018a) with the MODIS albedo (MCD43A3.006) dataset for summer of 2019. The LAI was derived from MOD15A2H.006 product in summer of 2019.

3. Methodology

In this study, a WRFM framework was developed to improve the estimation of hourly LSTs at a 1 km spatial resolution (Fig. 3). First, the WRF simulation was performed with the updated satellite-observed land surface properties. Second, the temporal pattern of WRF-simulated LSTs and spatial pattern of gap-filled 1 km daily 2 AM and 2 PM MODIS LST were integrated using the morphing technique (Belcher et al., 2005). Third, the performance of the WRF model and the capability of the WRF model and WRFM framework to capture the spatiotemporal variations of LSTs were evaluated using satellite and in situ LST observations. Finally, we investigated the spatiotemporal pattern of UHI effect using WRFM-generated LSTs. More details about each step are presented in the following sections.

3.1. WRF modeling and its configuration

WRF version 4.1 was used to simulate hourly LSTs for the study area and the SURFRAD site with identical model configuration. Specifically, we chose the Noah land surface model (Noah LSM) (Tewari et al., 2004) coupled with the single-layer urban canopy model (SLUCM) for the land surface; the Lin scheme (Chen and Sun, 2002) for microphysics; the Dudhia and RRTM schemes (Dudhia, 1989; Mlawer et al., 1997) for shortwave and longwave radiations, respectively; the Eta similarity scheme (Janjić, 1994) for surface layer; and the Mellor–Yamada–Janjic (MYJ) Scheme (Janjić, 1994) for the planetary boundary layer. Reanalysis data from the Global Forecast System (GFS) at the spatial resolution of 0.5 degrees and temporal resolution of 6 h ("Global Forecast System Analysis (GFS-ANL)") under both clear-sky and cloudy conditions were used as inputs for the initial and lateral boundary conditions. The simulations were performed from June 1st to August 31st, 2019, summer season in Iowa. The first 48 h of the simulation were used for spinning-up. The simulation results for the innermost domain (d03) were used to generate WRFM-LSTs and to investigate the spatiotemporal patterns of study area's thermal environment.

3.2. Morphing integration

The morphing technique described by Eqs. (1–3), developed by (Belcher et al., 2005) was adopted to integrate the temporal pattern of

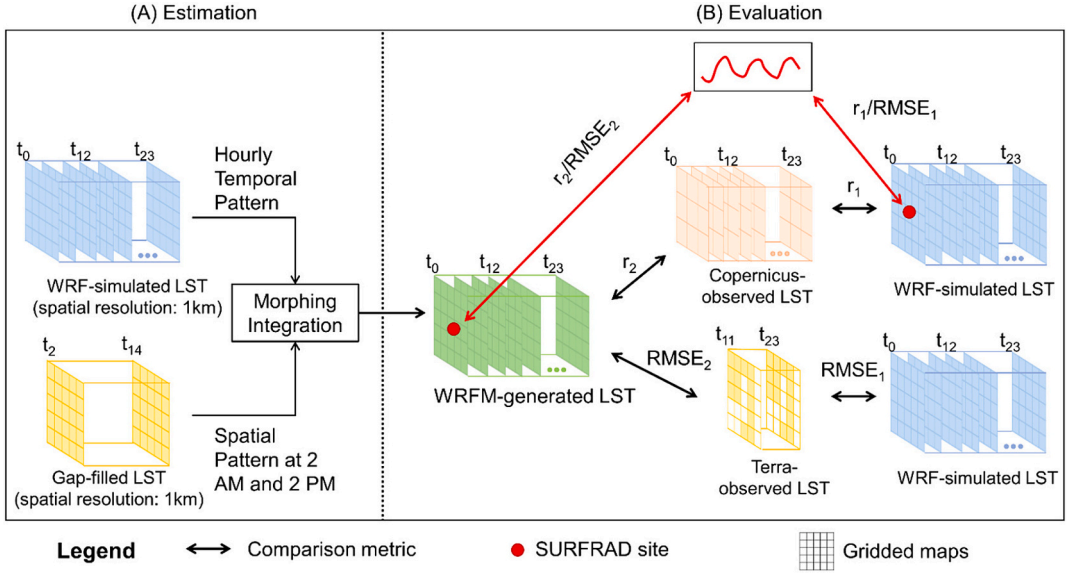

Fig. 3. The proposed framework with a combination of WRFM and satellite observations for estimating hourly LSTs at a 1 km resolution (A) and evaluating WRFM-generated LSTs based on satellite and in-situ LST observations (B).

WRF-simulated LSTs and spatial pattern of gap-filled MODIS LSTs. This method was used to adjust time series with two practical advantages. Firstly, the 'baseline climate' is reliable, which is from the WRF-simulated diurnal dynamic of LST during the study period that was driven by the background reanalysis climate data and physical parameterization schemes. By incorporating comprehensive atmospheric physics processes, WRF was able to generate reliable diurnal patterns of various meteorological variables (Fu et al., 2019). Second, the accuracy of spatial pattern of WRF-simulated LST was improved by integrating gap-filled LST from MODIS observation.

We utilized a morphing procedure (Fig. 4) consisting of the combination of shift and a stretch (Eq. (1)), performed on a daily basis. A shift by ΔX_d (Eq. (2)) was applied to the hourly WRF-LSTs (X_s), and a stretch by α_d was applied to the difference between hourly WRF-LSTs and the mean value calculated from WRF-LSTs at 2 AM and 2 PM. α_d (Eq. (3)) is the fractional change in the mean value calculated by WRF model and gap-filled MODIS-LST at 2 AM and 2 PM. After the combination of shift and stretch, the newly generated LST time series can preserve both the magnitude of satellite observed LSTs and the diurnal dynamic of WRF-simulated LSTs.

$$X = X_s + \Delta X_d + \alpha_d \times \left[X_s - (X_s)_d\right] \tag{1}$$

$$\Delta X_d = X_{mean} - (X_s)_d \tag{2}$$

$$\alpha_d = \frac{(X_{MODIS,2\ PM} - X_{WRF,2\ PM}) - (X_{MODIS,2\ AM} - X_{WRF,2\ AM})}{(X_{WRF,2\ PM} - X_{WRF,2AM})} \tag{3}$$

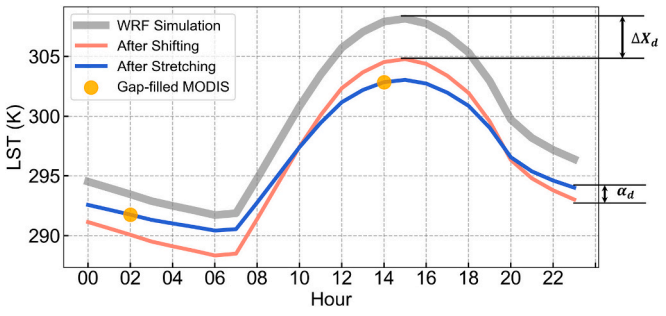

Fig. 4. An example of the morphing procedure.

where X_s is the hourly WRF-simulated LST, $(X_s)_d$ is the daily mean of hourly WRF-simulated LST, calculated as $\frac{X_{WRF,2\ PM}+X_{WRF,2\ AM}}{2}$, X_{mean} is the mean of gap-filled MODIS daily LST, calculated as $\frac{X_{MODIS,2\ PM}+X_{MODIS,2\ AM}}{2}$.

3.3. Accuracy assessment

We evaluated the performance of the WRF model and spatiotemporal patterns of the WRFM-generated LSTs by using satellite and station observations. Furthermore, we compared LST datasets obtained from conventional techniques, such as DTC and spatial downscaling, to evaluate the benefits of utilizing the WRFM framework. Statistical indicators (Eqs. (4–7)), including index of agreement (IoA), mean absolute error (MAE), RMSE, and Spearman's rank correlation coefficient (r), were calculated from observed and simulated temperature time series at the pixel level. RMSE and MAE were used to quantify the deviation between simulated and observed temperatures, and IoA and correlation coefficient r were used to determine the degree to which magnitude and signs of the observed temperatures are consistent with the simulated temperatures. Using the correlation coefficient r instead of Pearson's correlation coefficient (ρ), as a non-parametric rank statistical parameter, can reduce the influence of possible non-linearities between variables. Many previous studies (Crippa et al., 2019; Fu et al., 2019; Liu et al., 2021) have also used it to measure the consistency between WRF-simulated and satellite-observed variables. It should be noted that during the evaluation process, any pixels with missing values in either satellite or station observations were excluded.

$$IoA = 1 - \frac{\sum_{i=0}^{n}\left(T_{m,i} - T_{o,i}\right)^2}{\sum_{i=0}^{n}\left(\left|T_{m,i} - \mu_{T_o}\right| + \left|T_{o,i} - \mu_{T_o}\right|\right)^2} \tag{4}$$

$$\mathrm{MAE} = \frac{1}{n}\sum_{i=1}^{n}\left|T_{m,i} - T_{o,i}\right| \tag{5}$$

$$RMSE = \sqrt{\frac{\sum_{i=1}^{n}\left(T_{m,i} - T_{o,i}\right)^2}{n}} \tag{6}$$

$$r = \frac{\sum_{i=0}^{n}\left(T_{m,i} - \mu_{T_m}\right)\left(T_{o,i} - \mu_{T_o}\right)}{\left(\sum_{i=0}^{n}\left(T_{m,i} - \mu_{T_m}\right)^2 \sum_{i=0}^{n}\left(T_{o,i} - \mu_{T_o}\right)^2\right)^{1/2}} \tag{7}$$

where $T_{m,i}$ and $T_{o,i}$ are the modeling and observation temperature at time i; μ and σ are the mean and standard deviation of temperature.

First, we assessed the performance of the WRF model with updated land surface properties by comparing the simulated air temperature against observations at nine meteorological stations (Fig. 1C). IoA and MAE (Srivastava et al., 2015) for nine stations were calculated for WRF grids. Benchmarking of the performance of our evaluation against published studies to achieve the WRF simulation of air temperature based on IoA should be greater than 0.8 and MAE should be smaller than 2 °C (Bhati and Mohan, 2016).

Second, we assessed the performance of the WRFM framework using SURFRAD-observed and satellite-observed LSTs. In situ LST measurements at the SXF site were used to evaluate the performance of WRF simulation and WRFM framework under varying atmospheric conditions (i.e.,

clear-sky and cloud conditions). The determination of these conditions was accomplished through the utilization of a cloud mask derived from satellite products (i.e., Copernicus and MODIS). Hourly SURFRAD-observed LSTs over study period were compared to the corresponding WRF-simulated and WRFM-generated LSTs at the grid cell located in the SXF site. We further evaluated the capability of the WRFM framework into capturing the spatial and temporal variations of LSTs over the study region by comparing the WRFM generated LSTs with satellite-observed LSTs. In terms of spatial pattern, the RMSE in each WRF grid cell was calculated by comparing LST values from the WRFM generated LSTs with original MODIS Terra observations (10:30 AM and 10:30 PM). The aforementioned comparison was performed exclusively on days when four MODIS observations were available, thereby facilitating an independent evaluation by excluding LSTs that were generated in the process of the gap-filled LST product. This strategy ensures that the evaluation was conducted using a set of observations that were not influenced by the estimation techniques used in generating the gap-filled LST data. In terms of temporal pattern, the correlation coefficient r for each WRF grid was calculated by comparing averaged diurnal variations of LST from Copernicus observations and WRFM generated LSTs during the study period. Grids of the WRF simulation (1 km) were aggregated to 5 km to match the pixel size of the Copernicus LSTs.

Third, we assessed the effectiveness of the WRFM framework in capturing the diurnal and spatial patterns of LSTs by comparing the LSTs generated by WRFM with those generated by DTC model and spatial downscaling, respectively. The four-parameter DTC model used in this study was based on GOT01_0 model proposed by (Schädlich et al., 2001) and the input data was MODIS observations. This model was applied for nine days during the study period when more than 50 % MODIS pixels in the study areas have four clear-sky observations per day. Grids of the DTC modeled LST (1 km) were aggregated to 5 km and the correlation coefficient r and mean bias for each grid were calculated by comparing averaged diurnal variations of LST from Copernicus observations and DTC model for the study period. Next, we evaluated the effectiveness of the WRFM framework in capturing the diurnal pattern by comparing correlation coefficient r values between DTC-LSTs and Copernicus-LSTs, as well as between WRFM-LSTs and Copernicus-LSTs. The spatial downscaling approach used in this study was based on regression of principal components proposed by (Zakšek and Oštir, 2012). MODIS auxiliary data (i.e., land surface albedo, NDVI, EVI, emissivity), NLCD land cover data, and terrain data (i.e., slope, aspect) were used to downscale Copernicus LSTs for seven days when more than 90 % Copernicus pixels in the study areas have clear-sky observations. The RMSE was calculated by comparing LST values from the spatial downscaled LSTs and original MODIS observations for 10:30 AM and 10:30 PM (Terra) without missing values. Next, we evaluated the effectiveness of the WRFM framework in capturing the spatial pattern by comparing RMSE values between WRFM-LSTs and MODIS-LSTs, as well as between spatial downscaling-LSTs and MODIS-LSTs.

4. Results

4.1. Evaluation of the WRF modeling

The WRF model with updated land surface properties can well capture the hourly dynamics and magnitude of air temperatures compared to the station observations (Fig. 5). Specifically, the simulated air temperatures showed a strong agreement with the temporal dynamics of temperature records obtained from weather stations, as indicated by an IoA exceeding 0.92 for all weather stations. Meanwhile, the WRF simulation in this study demonstrated a competitive performance in estimating air temperature magnitude with a MAE (or RMSE) value smaller than 2 K (2.5 K) (Table 1). In general, the WRF simulation exhibited a high degree of agreement with station observations during nighttime, suggesting a better model performance at night. Cold biases on the order of 1–2 K were observed in daytime peak for all weather stations studied, which might be caused by model errors from the selected planetary boundary layer schemes (Hu et al., 2013; Hu et al., 2010).

The WRF simulation demonstrated certain limitations in accurately capturing spatial variations of LST across the study region and tended to exhibit a bias in magnitude. This was further evidenced by Fig. 6, which depicts the LSTs at approximately 2:00 AM local time on June 9 and August 19, 2019, as observed by the MODIS satellite and simulated by the WRF model. Although the spatial patterns of the WRF-simulated and MODIS-observed LSTs exhibited similarities, there were notable differences in their magnitudes, particularly in urban areas where the biases were more pronounced. Similar performance of WRF simulated LSTs was also reported in previous studies (Fu et al., 2019; Fu and Weng, 2018; Xia et al., 2017). The underestimation of LST was observed in urban areas on June 9, 2019, which might be caused by the setting of constant values of surface parameters in the coupled SLUCM model. Additionally, on August 19, there is a clear warm bias in the WRF-simulated LSTs compared with the observations. This bias may be potentially attributable to the model's inability to adequately capture local-scale factors and site-specific characteristics. These findings highlight the need for further refinement of the WRF-simulated LSTs to more accurately capture the spatial variations and magnitude of LST across the study area.

The performance of the WRF simulation in capturing the temporal pattern of LSTs was observed to be consistently good under varying weather conditions. However, the simulation demonstrated superior LST estimation in magnitude under clear-sky conditions compared to cloudy conditions. As demonstrated in Fig. 7A, the WRF simulation exhibited a good performance in capturing the temporal pattern of LST and estimating the magnitude of LST under clear sky, with a correlation coefficient r of 0.97 and RMSE of 2.73 K at the SURFRAD site. Under cloudy conditions, the WRF simulation was observed to perform well in capturing the temporal pattern of LST with a correlation coefficient r of 0.93 at the SURFRAD site (Fig. 7B). However, it is worth noting that the RMSE under cloudy conditions increased to 4.15 K, indicating a relatively poor performance in estimating the magnitude of LSTs compared to clear-sky conditions. According to Fig. 7C, the WRF simulation shows an overestimation of daytime LSTs, particularly at noon, under both clear and cloudy sky conditions. Furthermore, the extent of overestimation is more pronounced during cloudy sky conditions, resulting a higher RMSE.

4.2. Accuracy of the WRFM-generated LST

The implementation of the WRFM framework not only preserved the capability of the WRF simulation to capture temporal pattern of LST under varying weather conditions but also improved the estimation of LST magnitude, particularly under cloudy conditions (Fig. 7&8). Specifically, the WRFM can capture hourly LST under both clear and cloudy sky conditions, with RMSE of 2.63 and 3.75 K, respectively (Fig. 8 A&B).

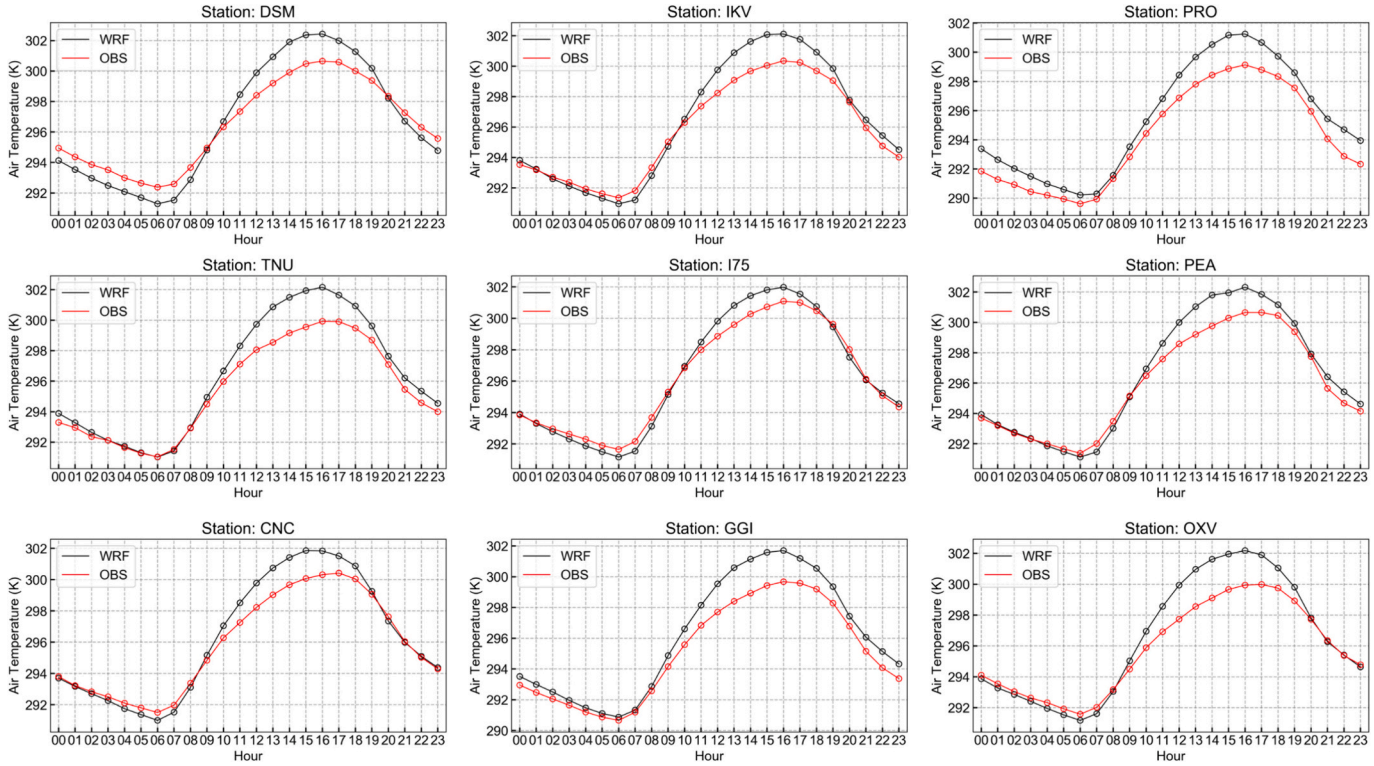

Fig. 5. The averaged diurnal variations (June 01–August 31, 2019) for air temperatures simulated from the WRF model and for temperature records from nine weather stations.

Table 1
Comparison of simulated air temperatures with those from the weather stations (2208 observations from June 1 to August 31, 2019).

Station ID	Latitude	Longitude	IoA	MAE (K)	RMSE (K)	Land Cover Type
IKV	41.69	−93.57	0.94	1.84	2.49	Developed, low intensity
CNC	41.02	−93.36	0.94	1.58	2.25	Developed, low intensity
DSM	41.53	−93.65	0.94	1.65	2.33	Developed, high intensity
GGI	41.71	−92.73	0.94	1.74	2.35	Developed, low intensity
OXV	41.30	−93.11	0.93	1.77	2.43	Developed, medium intensity
TNU	41.67	−93.02	0.94	1.80	2.41	Pasture
I75	41.05	−93.69	0.95	1.50	2.15	Cultivated crops
PEA	41.40	−92.94	0.94	1.70	2.41	Cultivated crops
PRO	41.83	−94.16	0.93	1.94	2.43	Cultivated crops

Moreover, the LSTs estimated by the WRFM framework still show a strong correlation with those obtained at the SURFRAD sites on an hourly basis and the estimated and measured LSTs align closely along the 1:1 line. The diurnal pattern of LST estimations was observed to align well with measurements after employing the WRFM framework under clear sky conditions (Fig. 8C). Additionally, the use of the WRFM framework resulted in an improvement in LST estimation accuracy under cloudy conditions, as evidenced by a decrease in the RMSE from 4.15 to 3.75 K. It is worth noting that the relatively large RMSE observed under cloudy conditions was a result of the underestimation of LST at nighttime, particularly during the early morning hours.

The WRFM can capture spatial variations and reduce bias in the magnitude of WRF-simulated LSTs. The LST observations obtained from the MODIS Terra satellite at around 10:30 AM and 10:30 PM were utilized to compare and evaluate the WRF-simulated and the WRFM-generated LSTs. The RMSE was calculated for both the WRF-MODIS and the WRFM-MODIS comparisons to evaluate the discrepancy of magnitude between the model-generated LSTs and the MODIS observations. In comparison to the RMSE value obtained from the WRF-MODIS comparison, the application of the morphing technique in the WRFM framework led to a substantial reduction in RMSE. Specifically, the maximum reduction in RMSE of approximately 5 K was observed in the northwestern areas of the study area during daytime (Fig. 9A&B). During nighttime, a similar reduction of approximately 3 K was observed in the northeastern areas of the study area (Fig. 9C&D). The analysis of the study area revealed a reduction in the average RMSE from 4.34 K to 2.89 K during daytime and from 4.12 K to 2.75 K during nighttime. In the southeastern region of the study area, although WRF-MODIS comparison exhibited relatively low RMSEs of about 3.5 K, the application of the morphing technique in WRFM framework resulted in a further reduction of RMSEs to less than 2.5 K. Overall, more than 80 % of the study areas exhibited RMSE of less than 3.3 K during the daytime and less than 3.1 K at night, when comparing the magnitude of WRFM-LST to those observed by MODIS. These findings suggest that the incorporation of the morphing technique enhances the accuracy of the WRF-simulated LSTs and improves the WRF model's ability to capture the spatial variations in LSTs over the study area.

The reliability of the WRF model in capturing the diurnal dynamics of LSTs was evident when compared to observations from the Copernicus satellite. Furthermore, the proposed WRFM framework has successfully maintained this reliability. The WRF simulation captured the diurnal variations in LSTs within the study region, as evidenced by a high correlation coefficient r exceeded 0.95 between the Copernicus-observed and WRF-simulated LSTs for the majority of grids within the study area (Fig. 10 A). The morphing technique within the WRFM framework demonstrated excellent performance in preserving temporal

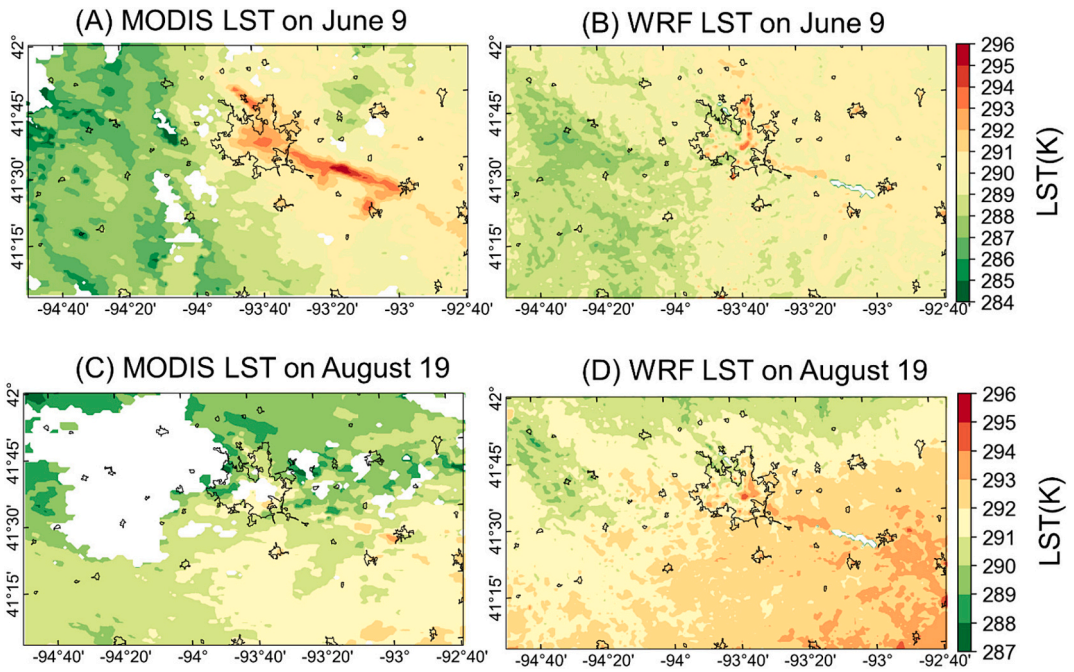

Fig. 6. LSTs simulated by the WRF/UCM model (B, D) and observed by MODIS (A, C) at 2:00 AM on June 9 and August 19, 2019. Note: White areas in Panel A and C were masked due to the low quality of the MODIS data product. The boundary of urban areas was marked in black.

variation of LSTs predicted by the WRF model. The majority of grid cells showed correlation coefficient r values exceeding 0.97 (Fig. 10 B), with negligible differences in correlation coefficient r values between the WRFM-generated and the WRF-simulated LSTs when compared with Copernicus observations, ranging from −0.016 to 0.06 (Fig. 10C). This outcome is theoretically expected, since one of the advantages offered by morphing integration process is to incorporate the reliable diurnal pattern derived from WRF model.

4.3. Comparison with previous methods

The spatial accuracy of the resulting WRFM LSTs from this study is better when compared with spatial downscaling LSTs reported in previous studies. The WRFM-generated LSTs show higher accuracies when compared with hourly LST at 1 km resolution obtained from spatial downscaling approach (Zakšek and Oštir, 2012). In certain rural areas (as shown in Fig. 11 A-E), the LSTs generated by WRFM and those derived from spatial downscaling exhibit similar RMSE when compared to MODIS observations, averaging around 3 K at 11 AM and 4 K at 11 PM. However, LSTs derived from spatial downscaling approach included outliers, resulting in a RMSE greater than 8 K for some parts of the study area. Particularly, RMSEs of the spatial-downscaled LSTs during daytime were large in urban areas despite the resulting coefficient of multiple determination from linear regression with auxiliary parameters mostly being larger than 0.8 (Fig. 11 C&F). A main reason for this poor performance by the spatial-downscaling method might be due to the limited ability of 5 km Copernicus observations to capture the magnitude of the LSTs difference between rural and urban area.

The diurnal pattern obtained from WRFM-generated LSTs in this study exhibits greater accuracy in comparison to that derived from the DTC model. The WRFM framework demonstrated better performance than DTC model with larger consistency with Copernicus observations and lower bias. Fig. 12 A&C show that the diurnal variation of LSTs captured by WRFM (with a correlation coefficient r larger than 0.97 for most of the grids) had higher correlations with Copernicus observations compared to those from the DTC model (with a correlation coefficient r larger than 0.93 for most of the grids). It should be noted that the LST values beyond the maximum and minimum observations in MODIS have been omitted from the evaluation to minimize the influence of outliers generated by the DTC model. Even after minimizing the influence of outliers, the spatial variation estimated by the DTC model was not as consistent with satellite observations as the proposed WRFM framework. In northern and eastern areas of the study area, correlation coefficient r values of the DTC model were found to be smaller than 0.94 and the application of the WRFM framework resulted in an increase in correlation coefficient r values ranging from 0.02 to 0.13 (Fig. 12 E). Overall, Copernicus grids with mean bias larger than 1.5 K were mostly observed in DTC-LSTs. The comparison between WRFM generated and Copernicus observed LSTs demonstrates that Copernicus grids situated in urban areas exhibited a relatively higher mean bias than those in rural areas (Fig. 12 B & D). This may be attributed to the complex urban environments within 5 km Copernicus, highlighting the importance of spatial resolution for improving the estimation of LST dynamics for complex landscapes.

4.4. Spatial and temporal patterns of LST

The WRFM-generated LSTs exhibit the capability to capture the UHI effect and reveal more detailed diurnal patterns of UHI in the study area compared to MODIS observations. For example, on August 4, 2019, the rural-urban gradient of LST was smallest at 9 AM, ranging from 1 to 2 K (Fig. 13A). After 9 AM, urban LSTs increased more quickly than rural LSTs and reached a maximum of ~40 °C at 2 PM, implying a strong warming effect of impervious surfaces after the absorption of solar radiation and anthropogenic heat released from human activities (e.g., transportation and building energy consumption). After 5 PM, the LSTs in rural areas decreased more rapidly than urban areas and reached a minimum of around 12 °C at 6 AM of the following day. The ability of MODIS observations to provide a detailed evolution of the UHI effect is limited due to missing values caused by clouds and the limited number of observations per day (Fig. 13B). It is worth noting that the WRFM-generated LSTs mainly reflect clear-sky conditions due to the integration of gap-filled clear-sky 1 km daily LST. By combining the WRFM framework with an all-weather gap-filled LST dataset, analyzing UHI variations becomes feasible.

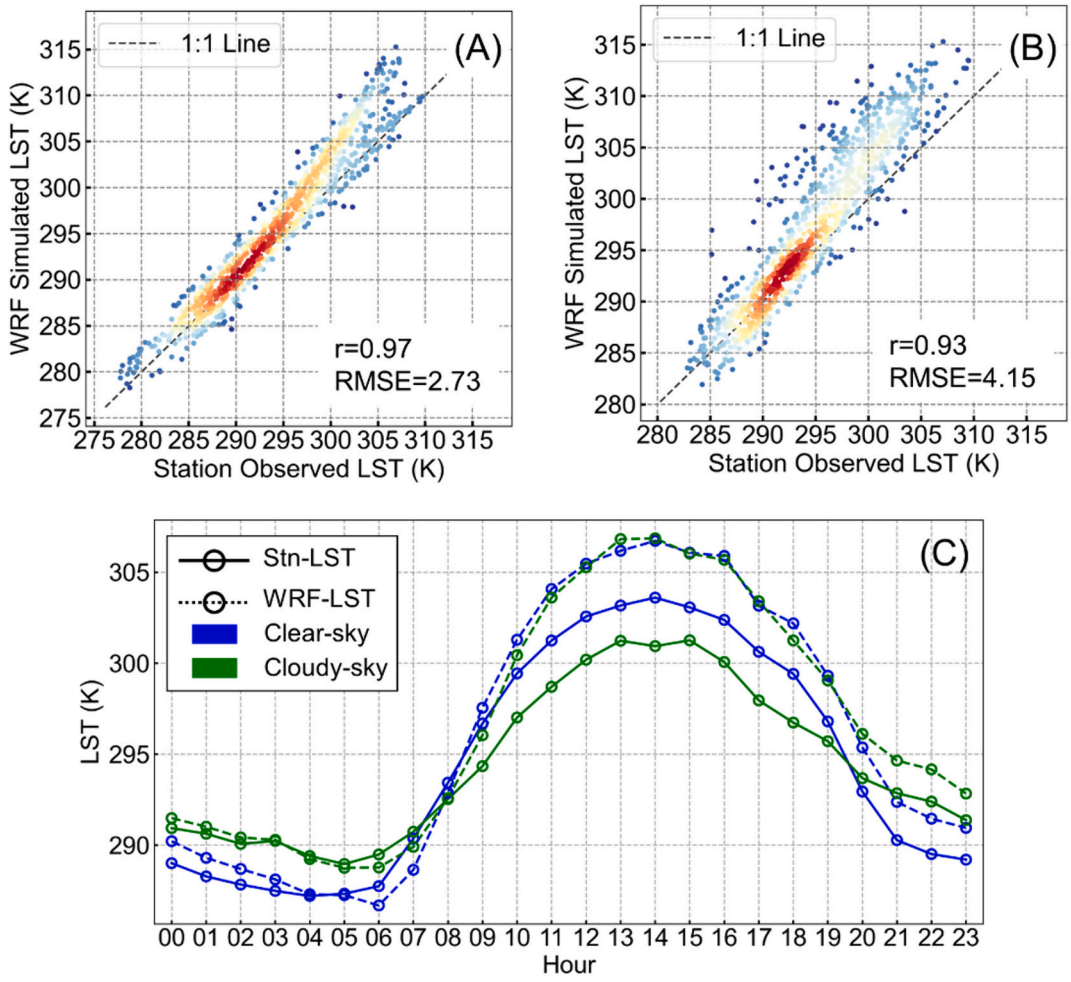

Fig. 7. The scatter density plots between SURFRAD-observed and WRF-simulated LSTs during the study period under clear (A) and cloudy sky conditions (B). Red color indicates higher density of points, blue color lower density. The averaged diurnal variations for LSTs from SURFRAD (Stn-LST) measurements and WRF (WRF-LST) simulations over the study period (C). (For interpretation of the references to color in this figure legend, the reader is referred to the web version of this article.)

5. Discussion

The complementary gap-filled MODIS observed and WRF-simulated LSTs can be integrated to improve hourly LSTs estimations at 1 km resolution. In the 1 km daily gap-filled MODIS LST dataset, missing values induced by clouds in the original MODIS data were effectively and efficiently filled using a spatiotemporal fitting algorithm. Although the gap-filled MODIS LST dataset only provided daily mid-daytime and mid-nighttime LSTs, it had the advantage of spatial details and accuracy. The WRF model has been used to estimate LSTs at high spatial and temporal resolutions. Comparing with satellite observations, we found that the WRF simulation exhibited superior capability in capturing diurnal variations of LSTs with correlation coefficient r greater than 0.92. However, the simulated LSTs tended to have a bias in the magnitude with a wide range of RMSE from 2 K to 7 K. By integrating complementary gap-filled MODIS and WRF-simulated LSTs, the morphing technique serves as a useful tool to generate LSTs with an improved accuracy of magnitude based on MODIS-observations and preserve temporal dynamics predicted by the WRF model. Therefore, the proposed WRFM framework in this study benefits from both attributes.

The WRFM framework, with its physically based weather modeling heritage, has demonstrated its ability to generate more reliable and refined diurnal dynamics of LST compared to the DTC model or the spatial downscaling approach. Firstly, the diurnal dynamics of LST derived from the DTC model are typically modeled with piecewise functions (e.g., a simple sine or cosine function or harmonic series) and its performance highly depends on the number of parameters considered in the DTC model. The inclusion of a higher number of parameters in the DTC model necessitates a greater number of LST observations within a day for accurate prediction. For example, in this study, the GOT01_0 model, a DTC model with four free parameters, was investigated. However, it was found that this model exhibits limited capability in capturing the variations of LSTs, leading to occurrence of outlier data points that fell outside the range of observed LSTs on certain days. Secondly, in terms of spatial downscaling approach, the diurnal dynamics of LST were derived from satellites with a high temporal resolution (i.e., hourly) but low spatial resolution (i.e., 5 km). This limitation hinders the ability to generate refined temporal patterns at a 1 km scale and also fails to mitigate the influence of cloud. Specifically, each Copernicus pixel encompasses a minimum of 25 WRF grid cells that may represent distinct urban land use types (e.g., low/high density residential, commercial, etc.). Moreover, the integrity of diurnal patterns derived from Copernicus observations was impacted by cloud and it is not ideal to obtain whole diurnal pattern for each day. Although using an all-sky hourly LST product at 5 km resolution (Jia et al., 2023) may mitigate the impact of cloud, the ability to generate more precise temporal patterns at a 1 km scale is still limited by its spatial resolution. In contrast to the aforementioned approaches, the proposed WRFM framework exhibits the capability to effectively capture the diurnal dynamics of LST at a fine spatial resolution by integrating WRF model. This integration leverages the advantages of the WRF model, which is coupled with readily available physical parameterization and diverse

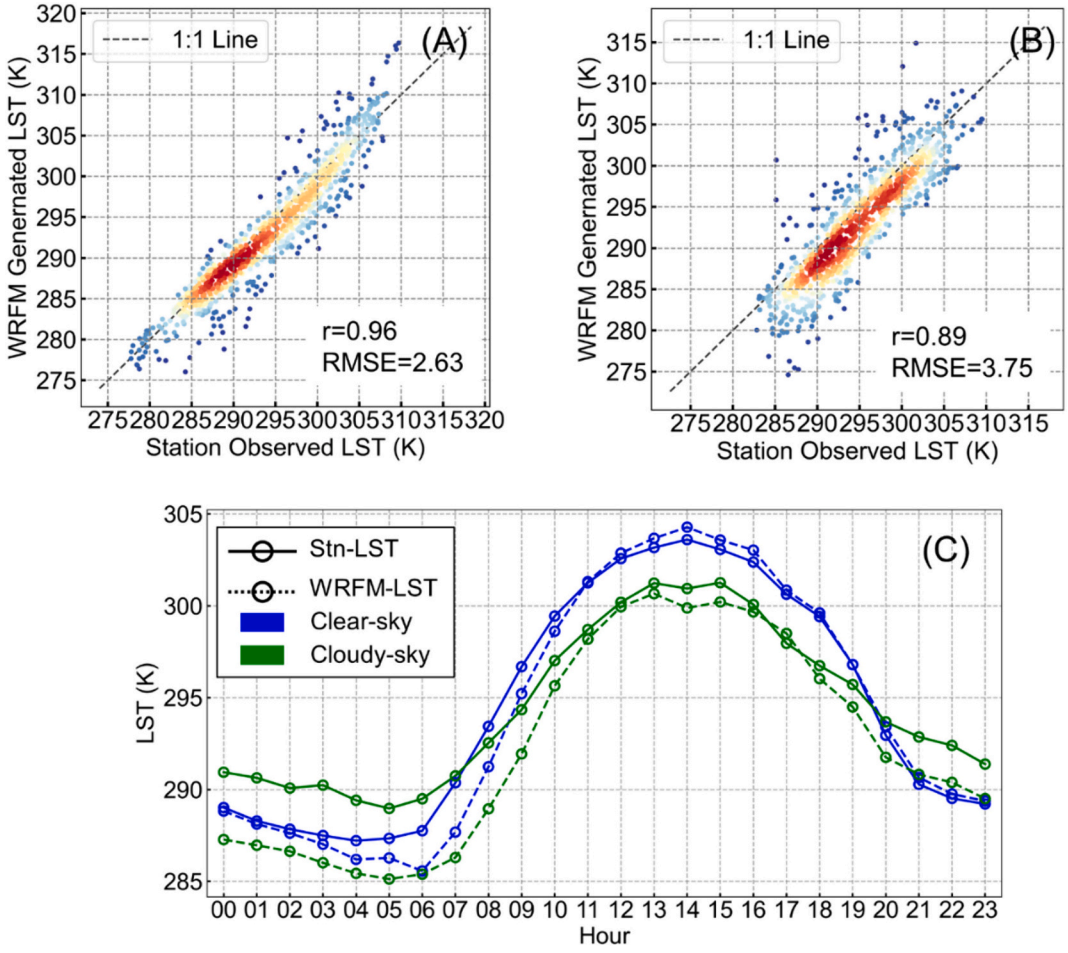

Fig. 8. The scatter density plots between SURFRAD-observed and WRFM-generated LSTs during the study period under clear (A) and cloudy sky conditions (B). Red color indicates higher density of points, blue color lower density. The averaged diurnal variations for LSTs from SURFRAD (Stn-LST) measurements and WRFM (WRFM-LST) framework over the study period (C). (For interpretation of the references to color in this figure legend, the reader is referred to the web version of this article.)

land cover types, enabling the characterization of LST's diurnal pattern at a resolution of 1 km in an effectively way. Additionally, WRF model can simulate diurnal pattern of LST under both clear-sky and cloudy conditions with its advanced ability to parameterize microphysical process and planetary boundary layer conditions (Fu et al., 2019).

The proposed WRFM framework uses more and up-to-date land surface parameters from in situ and satellite observations, thus can generate more reliable spatial pattern of LSTs compared to those from the spatial downscaling approach or original WRF model. Firstly, when using a spatial downscaling approach, a large number of land surface parameters relevant to LSTs must be manually collected and incorporated to accurately characterize spatial variations in LSTs. In contrast, the WRFM framework incorporates a wide range of land surface parameters in a highly efficient manner. This is made possible by leveraging the extensive collection of static datasets provided by the WRF model community, which includes essential land features such as soil temperatures, topology, and soil types. Secondly, with the updated satellite-observed land surface properties, the performance of the WRF model can meet the evaluation benchmark for 2-m air temperature, but the simulated LST still showed bias in the magnitude when compared with the original MODIS LSTs. Further tuning LST-related parameters (e.g., turbulent transfer coefficient (Vahmani and Hogue, 2014) and the emissivity of LULC) in the WRF model might be able to further improve the accuracy of LST. However, such process is computationally expensive because a complete analysis of the model sensitivity to the changes of LST-related parameters in the WRF model needs an extensive number of model runs. The gap-filled MODIS LSTs provided a reliable spatial pattern of daily LSTs for the proposed WRFM framework.

The proposed WRFM framework, supported by a large community of users of the WRF model and a simple morphing integration algorithm, offers a straightforward approach to generate LSTs and its dynamics for various regions. This represents an improvement over existing sophisticated fusion methods. Various fusion methods have been proposed to estimate LSTs at high spatiotemporal resolutions using multi-scale polar-orbiting and geostationary satellite observations (Adeniran et al., 2024; Long et al., 2020; Ma et al., 2022; Quan et al., 2018; Wu et al., 2015; Wu et al., 2013; Zhao et al., 2020). However, these methods are not satisfactory due to the following reasons: 1) the application of these methods over large areas can be quite challenging due to their structures and procedures, low computing efficiencies, and the need for specific hypothesis; 2) potential high uncertainties due to accumulated uncertainties and spatiotemporal mismatching issues among multi-source datasets; and 3) the availability of data sources and source codes for models may not always be publicly available. Moreover, deep learning algorithms, such as convolutional neural network (CNN) (Wang and Huang, 2024; Yu et al., 2023) and dynamic multilayer perceptron (DyNet) (Guo et al., 2024), have also been used for fusing LST data, mainly on daily frequency and with a spatial resolution of finer than 1 km. Despite their advantages, deep learning algorithms may not be suitable for large-scale applications as their performance is highly dependent on the characteristics of the study areas, leading to a poor universality. On the contrary, the proposed WRFM framework in this

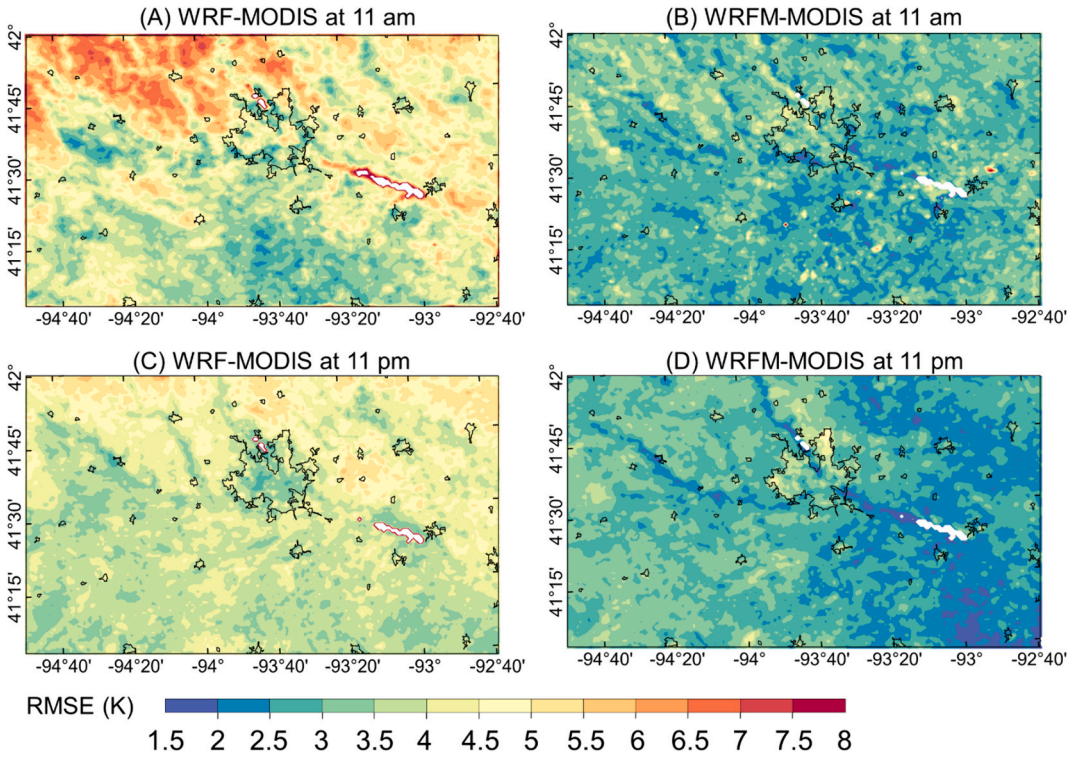

Fig. 9. The RMSE between the WRF simulated (A&C) and WRFM generated (B&D) LSTs according to MODIS observed LSTs at 11 am and 11 pm, respectively. The boundary of urban areas was marked in black.

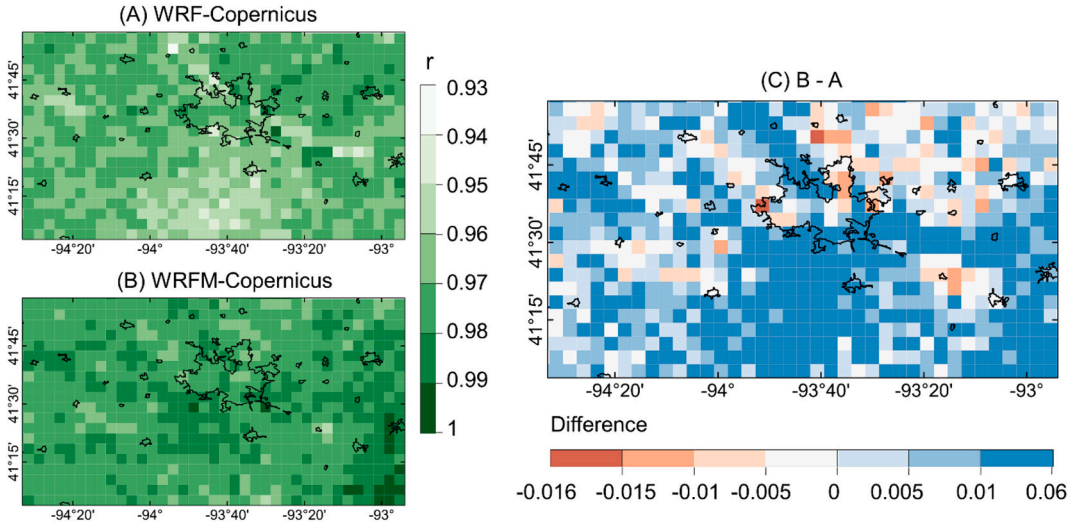

Fig. 10. The correlation coefficient r between the WRF simulated (A) and WRFM generated (B) LSTs, and their difference (WRFM-WRF) (C) as compared with Copernicus observed LSTs. The boundary of urban areas was marked in black.

study offers several advantages. Firstly, the proposed framework is suitable for large-scale applications due to its ease of implementation, high efficiency, and robustness. Secondly, the spatial resolution of the LSTs obtained from both WRF outputs and MODIS observations is same, which eliminates any potential issues related to scale effects. Thirdly, the WRF model and the inputs required for the proposed framework are public available. As a state-of-the-art mesoscale numerical weather prediction system, the WRF model has a large worldwide community of registered users and support forum, thereby facilitating swift resolution of issues that users may encounter. The proposed framework can incorporate publicly available seamless LST products, such as the gap-filled clear-sky 1 km daily LST (Zhang et al., 2022d) used in this study, to improve LSTs produced by the WRF model. Thus, the proposed WRFM framework, in combination with the use of gap-filled LSTs, holds great potential for studying the effects of UHIs and for conducting other research related to urban systems.

The resulting hourly LSTs at a high spatial resolution were able to provide more accurate spatial and temporal details of thermal environment of the diverse study area in this study when compared to other available datasets. Specifically, more accurate spatial pattern of rural-urban thermal gradient can be obtained from the WRFM-generated LSTs. In addition, compared to MODIS LSTs, hourly patterns of UHI effect can be examined at a 1 km resolution. Overall, the WRFM-generated LSTs with good accuracies and high spatiotemporal

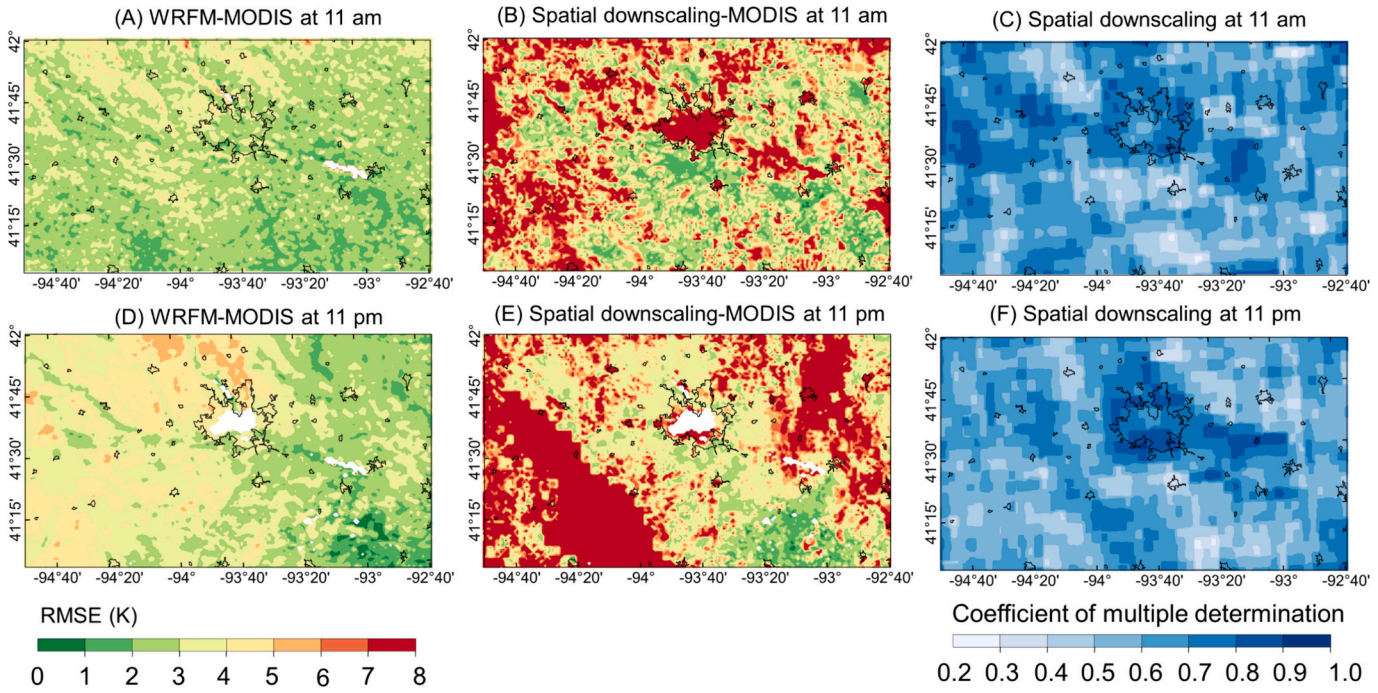

Fig. 11. RMSEs of the WRFM generated (A: 11 am, D: 11 pm) and spatially downscaled (B: 11 am, E: 11 pm) LSTs evaluated based on MODIS observed-LSTs and the corresponding coefficients of multiple determination of the spatial downscaling method (C: 11 am, F: 11 pm). Note: Copernicus observations for 8 days (6/7, 6/8, 6/10, 6/13, 7/19, 7/23, 8/27, 8/28) with greater than 90 % clear sky were selected for this evaluation. Pixels with less than three clear-sky observations were excluded in RMSE calculation. The boundaries of urban areas were marked in black.

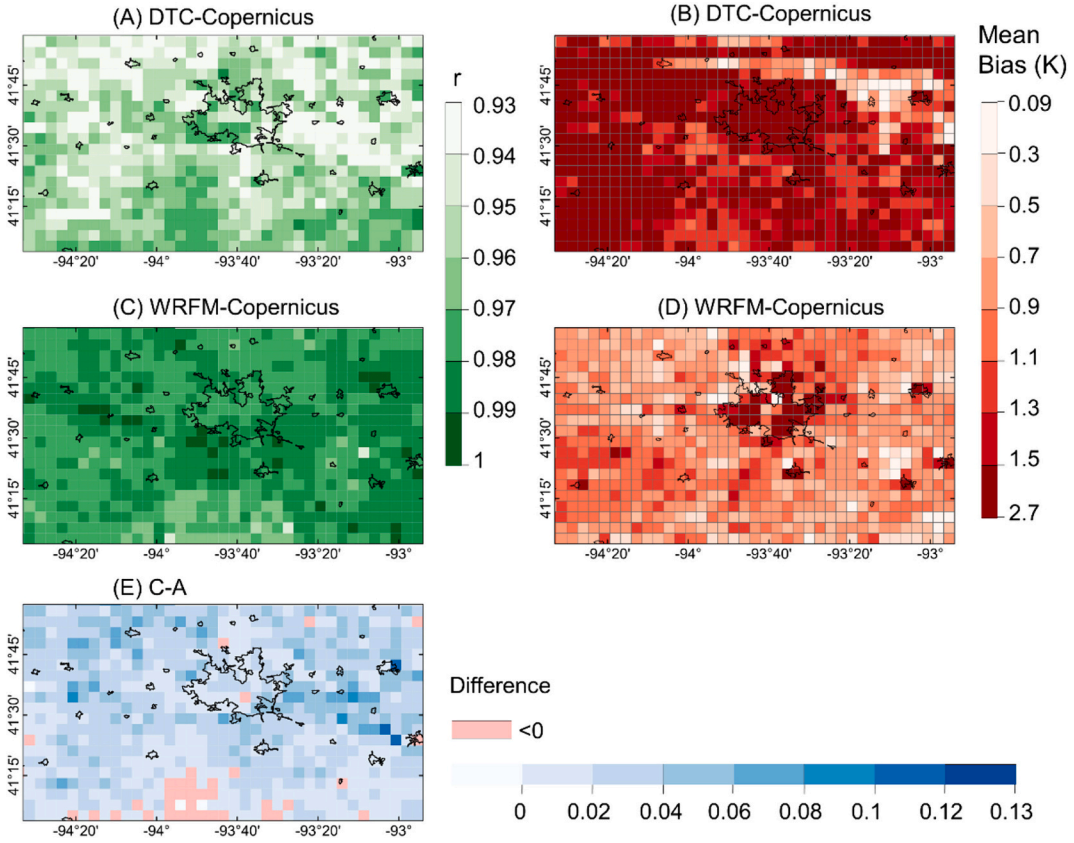

Fig. 12. The correlation coefficient r and mean bias between the DTC fitted (A&B) and WRFM generated (C&D) LSTs with Copernicus observed LSTs and the difference of between correlation coefficient r (E). Note: MODIS observations for 9 days (6/7, 6/8, 7/10, 7/12, 7/19, 7/23, 8/8, 8/27, 8/28) with larger than 50 % clear-sky were selected to conduct this evaluation. The boundary of urban areas was marked in black.

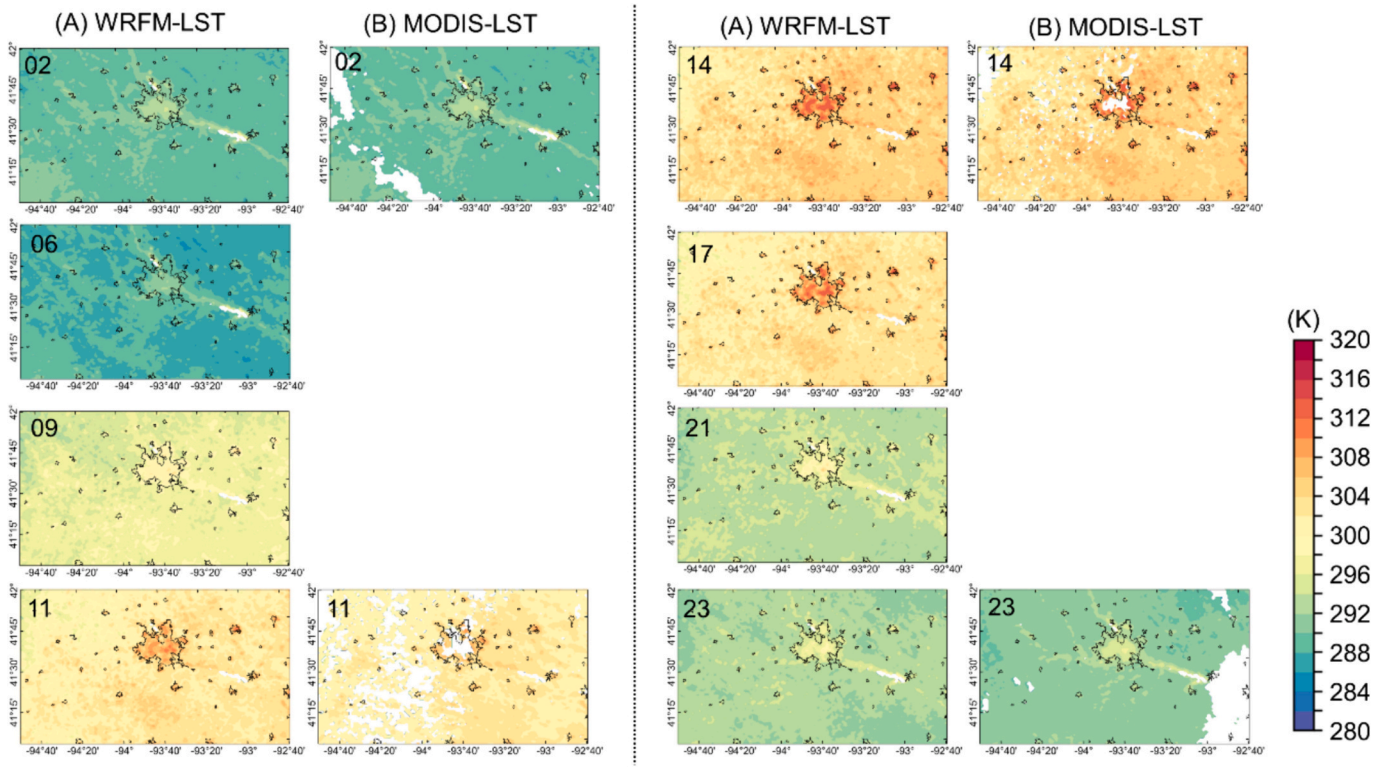

Fig. 13. The spatial pattern of hourly LSTs on August 4, 2019 from WRFM framework (A) and MODIS observation (B). Note: White areas in Panel A were masked by water body. White areas in Panel B were masked per the quality flag provided in the MODIS data product.

resolutions can offer better information about LSTs to researchers and policymakers, for understanding diurnal evolution of thermal environment and further locating regions that require urban heat mitigation strategies.

6. Conclusions

An improved understanding of the diurnal dynamics in LSTs, especially over urban domain, has been hindered due to the limitation in spatial and temporal resolutions and missing observations in satellite observations and potential bias from weather modeling. In this study, we developed a practical framework (named WRFM) that benefits from the combined features of weather modeling and satellite observations to estimate hourly 1 km LSTs. The proposed framework integrates temporal features of the WRF model with the spatial pattern of gap-filled 1 km daily MODIS LST observations to generate an improved LST product. The framework consists of two steps. First, the updated land surface datasets were used in WRF simulation to generate gridded LST data. Second, the temporal pattern of WRF-simulated and spatial pattern of observed and gap-filled LSTs were integrated using the morphing technique. The improved LSTs with spatial and temporal details can be used to reveal the thermal environment that consists of a diverse and complex LULC and urbanization levels. Compared with previous studies, the proposed framework can generate high-accuracy and resolution hourly LSTs by combining the complementary attributes of LSTs from satellite observations (i.e., spatial information) and the physically based WRF (i.e., diurnal dynamics) simulations.

Using eight counties in Iowa as the study area, the results suggest that the temporal pattern of LSTs can be well captured by the WRF model with the updated land surface properties. Further utilization of the morphing technique can reduce the bias in the magnitude between WRF-simulated and MODIS observed LSTs while still maintaining temporal pattern of WRF-simulated LSTs. The resultant data can be used to study the spatial pattern of LSTs and their hotspots at an hourly scale. The improved spatiotemporal LSTs can also improve our understanding of the diurnal evolution of thermal environment in urban, sub-urban, and rural areas, that are useful to researcher, policymakers, and city planners for understanding and mitigating the effects of UHI on human health (i.e., heat stress) and other socioeconomic activities (e.g., energy demand, transportation).

CRediT authorship contribution statement

Wei Chen: Writing – original draft, Validation, Software, Methodology, Investigation, Formal analysis. **Yuyu Zhou:** Writing – review & editing, Supervision, Methodology, Funding acquisition, Conceptualization. **Ulrike Passe:** Writing – review & editing. **Tao Zhang:** Writing – review & editing. **Chenghao Wang:** Writing – review & editing. **Ghassem R. Asrar:** Writing – review & editing. **Qi Li:** Writing – review & editing. **Huidong Li:** Writing – review & editing.

Declaration of competing interest

The authors declare that they have no known competing financial interests or personal relationships that could have appeared to influence the work reported in this paper.

Data availability

No data was used for the research described in the article.

Acknowledgements

This work was supported by the National Science Foundation [grant numbers 1855902] and The University of Hong Kong HKU-100 Scholars Fund.

References

Adeniran, I.A., Nazeer, M., Wong, M.S., Zhu, R., Yang, J., Chan, P.-W., 2024. Improved fusion model for generating hourly fine scale land surface temperature data under all-weather condition. Int. J. Appl. Earth Obs. Geoinf. 131, 103981.

Aires, F., Prigent, C., Rossow, W.B., 2004. Temporal interpolation of global surface skin temperature diurnal cycle over land under clear and cloudy conditions. J. Geophys. Res. Atmos. 109.

Augustine, J.A., DeLuisi, J.J., Long, C.N., 2000. SURFRAD–A national surface radiation budget network for atmospheric research. Bull. Am. Meteorol. Soc. 81, 2341–2358.

Belcher, S.E., Hacker, J.N., Powell, D.S., 2005. Constructing design weather data for future climates. Build. Serv. Eng. Res. Technol. 26, 49–61.

Bhati, S., Mohan, M., 2016. WRF model evaluation for the urban heat island assessment under varying land use/land cover and reference site conditions. Theor. Appl. Climatol. 126, 385–400.

Chen, S.-H., Sun, W.-Y., 2002. A one-dimensional time dependent cloud model. J. Meteorol. Soc. Japan Ser. II 80, 99–118.

Chen, F., Mitchell, K., Schaake, J., Xue, Y., Pan, H., Koren, V., Duan, Q.Y., Ek, M., Betts, A., 1996. Modeling of land surface evaporation by four schemes and comparison with FIFE observations. J. Geophys. Res. Atmos. 101, 7251–7268.

Chen, F., Kusaka, H., Tewari, M., Bao, J.W., Hirakuchi, H., 2004. Utilizing the coupled WRF/LSM/urban modeling system with detailed urban classification to simulate the urban heat island phenomena over the greater Houston area. In: Fifth Symposium on the Urban Environment. American Meteorological Society Vancouver, BC, Canada, pp. 9–11.

Chen, F., Kusaka, H., Bornstein, R., Ching, J., Grimmond, C.S.B., Grossman-Clarke, S., Loridan, T., Manning, K.W., Martilli, A., Miao, S., 2011. The integrated WRF/urban modelling system: development, evaluation, and applications to urban environmental problems. Int. J. Climatol. 31, 273–288.

Chen, F., Yang, X., Zhu, W., 2014. WRF simulations of urban heat island under hot-weather synoptic conditions: the case study of Hangzhou City, China. Atmos. Res. 138, 364–377.

Crippa, P., Sullivan, R.C., Thota, A., Pryor, S.C., 2019. Sensitivity of simulated aerosol properties over eastern North America to WRF-Chem parameterizations. J. Geophys. Res. Atmos. 124, 3365–3383.

Di, Z., Duan, Q., Wang, C., Ye, A., Miao, C., Gong, W., 2018. Assessing the applicability of WRF optimal parameters under the different precipitation simulations in the greater Beijing area. Clim. Dyn. 50, 1927–1948.

Duan, S.-B., Li, Z.-L., Wang, N., Wu, H., Tang, B.-H., 2012. Evaluation of six land-surface diurnal temperature cycle models using clear-sky in situ and satellite data. Remote Sens. Environ. 124, 15–25.

Duan, S.-B., Li, Z.-L., Tang, B.-H., Wu, H., Tang, R., 2014. Direct estimation of land-surface diurnal temperature cycle model parameters from MSG–SEVIRI brightness temperatures under clear sky conditions. Remote Sens. Environ. 150, 34–43.

Dudhia, J., 1989. Numerical study of convection observed during the winter monsoon experiment using a mesoscale two-dimensional model. J. Atmos. Sci. 46, 3077–3107.

Freitas, S.C., Trigo, I.F., Macedo, J., Barroso, C., Silva, R., Perdigão, R., 2013. Land surface temperature from multiple geostationary satellites. Int. J. Remote Sens. 34, 3051–3068.

Fu, P., Weng, Q., 2018. Responses of urban heat island in Atlanta to different land-use scenarios. Theor. Appl. Climatol. 133, 123–135.

Fu, P., Xie, Y., Weng, Q., Myint, S., Meacham-Hensold, K., Bernacchi, C., 2019. A physical model-based method for retrieving urban land surface temperatures under cloudy conditions. Remote Sens. Environ. 230, 111191.

Fullhart, A.T., Nearing, M.A., McGehee, R.P., Weltz, M.A., 2020. Temporally downscaling a precipitation intensity factor for soil erosion modeling using the NOAA-ASOS weather station network. Catena (Amst) 194, 104709.

Göttsche, F.-M., Olesen, F.S., 2001. Modelling of diurnal cycles of brightness temperature extracted from METEOSAT data. Remote Sens. Environ. 76, 337–348.

Guo, S., Li, M., Li, Y., Chen, J., Zhang, H.K., Sun, L., Wang, J., Wang, R., Yang, Y., 2024. The improved U-STFM: a deep learning-based nonlinear spatial-temporal fusion model for land surface temperature downscaling. Remote Sens. 16, 322.

Gutman, G., Ignatov, A., 1998. The derivation of the green vegetation fraction from NOAA/AVHRR data for use in numerical weather prediction models. Int. J. Remote Sens. 19, 1533–1543.

He, J.J., Yu, Y., Yu, L.J., Liu, N., Zhao, S.P., 2017. Impacts of uncertainty in land surface information on simulated surface temperature and precipitation over China. Int. J. Climatol. 37, 829–847.

He, X., Li, Y., Wang, X., Chen, L., Yu, B., Zhang, Y., Miao, S., 2019. High-resolution dataset of urban canopy parameters for Beijing and its application to the integrated WRF/urban modelling system. J. Clean. Prod. 208, 373–383.

Hong, F., Zhan, W., Göttsche, F.-M., Liu, Z., Zhou, J., Huang, F., Lai, J., Li, M., 2018. Comprehensive assessment of four-parameter diurnal land surface temperature cycle models under clear-sky. ISPRS J. Photogramm. Remote Sens. 142, 190–204.

Hu, X.-M., Nielsen-Gammon, J.W., Zhang, F., 2010. Evaluation of three planetary boundary layer schemes in the WRF model. J. Appl. Meteorol. Climatol. 49, 1831–1844.

Hu, X., Klein, P.M., Xue, M., 2013. Evaluation of the updated YSU planetary boundary layer scheme within WRF for wind resource and air quality assessments. J. Geophys. Res. Atmos. 118, 10–490.

Hu, L., Sun, Y., Collins, G., Fu, P., 2020. Improved estimates of monthly land surface temperature from MODIS using a diurnal temperature cycle (DTC) model. ISPRS J. Photogramm. Remote Sens. 168, 131–140.

Hu, J., Yang, Y., Zhou, Y., Zhang, T., Ma, Z., Meng, X., 2022. Spatial patterns and temporal variations of footprint and intensity of surface urban heat island in 141 China cities. Sustain. Cities Soc. 77, 103585.

Huang, F., Zhan, W., Duan, S.-B., Ju, W., Quan, J., 2014. A generic framework for modeling diurnal land surface temperatures with remotely sensed thermal observations under clear sky. Remote Sens. Environ. 150, 140–151.

Jaber, S.M., Abu-Allaban, M.M., 2020. MODIS-based land surface temperature for climate variability and change research: the tale of a typical semi-arid to arid environment. Eur. J. Remote Sens. 53, 81–90.

Janjić, Z.I., 1994. The step-mountain eta coordinate model: further developments of the convection, viscous sublayer, and turbulence closure schemes. Mon. Weather Rev. 122, 927–945.

Ji, D., Dong, W., Hong, T., Dai, T., Zheng, Z., Yang, S., Zhu, X., 2018. Assessing parameter importance of the weather research and forecasting model based on global sensitivity analysis methods. J. Geophys. Res. Atmos. 123, 4443–4460.

Jia, A., Liang, S., Wang, D., Ma, L., Wang, Z., Xu, S., 2023. Global hourly, 5 km, all-sky land surface temperature data from 2011 to 2021 based on integrating geostationary and polar-orbiting satellite data. Earth Syst. Sci. Data 15, 869–895.

Jiang, X., Wiedinmyer, C., Chen, F., Yang, Z., Lo, J.C., 2008. Predicted impacts of climate and land use change on surface ozone in the Houston, Texas, area. J. Geophys. Res. Atmos. 113.

Jiménez, M.A., Ruiz, A., Cuxart, J., 2015. Estimation of cold pool areas and chilling hours through satellite-derived surface temperatures. Agric. For. Meteorol. 207, 58–68.

Kirthiga, S.M., Patel, N.R., 2018. Impact of updating land surface data on micrometeorological weather simulations from the WRF model. Atmósfera 31, 165–183.

Kurkowski, N.P., Stensrud, D.J., Baldwin, M.E., 2003. Assessment of implementing satellite-derived land cover data in the eta model. Weather Forecast. 18, 404–416.

Li, Z.-L., Tang, B.-H., Wu, H., Ren, H., Yan, G., Wan, Z., Trigo, I.F., Sobrino, J.A., 2013. Satellite-derived land surface temperature: current status and perspectives. Remote Sens. Environ. 131, 14–37.

Li, Xiaoma, Zhou, Y., Asrar, G.R., Imhoff, M., Li, Xuecao, 2017. The surface urban heat island response to urban expansion: a panel analysis for the conterminous United States. Sci. Total Environ. 605–606, 426–435. https://doi.org/10.1016/j.scitotenv.2017.06.229.

Li, Q., Ma, M., Wu, X., Yang, H., 2018a. Snow cover and vegetation-induced decrease in global albedo from 2002 to 2016. J. Geophys. Res. Atmos. 123, 124–138.

Li, X., Zhou, Y., Asrar, G.R., Zhu, Z., 2018b. Creating a seamless 1 km resolution daily land surface temperature dataset for urban and surrounding areas in the conterminous United States. Remote Sens. Environ. 206, 84–97.

Li, W., Zhou, Y., Cetin, K.S., Yu, S., Wang, Y., Liang, B., 2018c. Developing a landscape of urban building energy use with improved spatiotemporal representations in a cool-humid climate. Build. Environ. 136, 107–117.

Li, H., Zhou, Y., Li, X., Meng, L., Wang, X., Wu, S., Sodoudi, S., 2018d. A new method to quantify surface urban heat island intensity. Sci. Total Environ. 624, 262–272.

Li, H., Zhou, Y., Wang, X., Zhou, X., Zhang, H., Sodoudi, S., 2019. Quantifying urban heat island intensity and its physical mechanism using WRF/UCM. Sci. Total Environ. 650, 3110–3119.

Li, X., Zhou, Y., Hejazi, M., Wise, M., Vernon, C., Iyer, G., Chen, W., 2021. Global urban growth between 1870 and 2100 from integrated high resolution mapped data and urban dynamic modeling. Commun. Earth Environ. 2, 1–10.

Li, H., Zhou, Y., Jia, G., Zhao, K., Dong, J., 2022. Quantifying the response of surface urban heat island to urbanization using the annual temperature cycle model. Geosci. Front. 13, 101141.

Liu, C., Ikeda, K., Rasmussen, R., Barlage, M., Newman, A.J., Prein, A.F., Chen, F., Chen, L., Clark, M., Dai, A., 2017. Continental-scale convection-permitting modeling of the current and future climate of North America. Clim. Dyn. 49, 71–95.

Liu, X., Zhou, Y., Yue, W., Li, X., Liu, Y., Lu, D., 2020. Spatiotemporal patterns of summer urban heat island in Beijing, China using an improved land surface temperature. J. Clean. Prod. 257, 120529.

Liu, X., Zhang, L., Zhang, Z., Zhao, T., Zou, L., 2021. Ultra short term wind power prediction model based on WRF wind speed prediction and catboost. In: IOP Conference Series: Earth and Environmental Science. IOP Publishing, p. 12001.

Long, D., Yan, L., Bai, L., Zhang, C., Li, X., Lei, H., Yang, H., Tian, F., Zeng, C., Meng, X., 2020. Generation of MODIS-like land surface temperatures under all-weather conditions based on a data fusion approach. Remote Sens. Environ. 246, 111863.

Lu, L., Zhou, X.M., 2021. A four-parameter model for estimating diurnal temperature cycle from MODIS land surface temperature product. J. Geophys. Res. Atmos. 126 e2020JD033855.

Ma, H.-Y., Klein, S.A., Xie, S., Morcrette, C.J., Van Weverberg, K., Zhang, Y., Lo, M.-H., 2015. CAUSES: clouds above the United States and errors at the surface. In: AGU Fall Meeting Abstracts, pp. A41J–0209.

Ma, J., Shen, H., Wu, P., Wu, J., Gao, M., Meng, C., 2022. Generating gapless land surface temperature with a high spatio-temporal resolution by fusing multi-source satellite-observed and model-simulated data. Remote Sens. Environ. 278, 113083.

Meng, X., Lyu, S., Zhang, T., Zhao, L., Li, Z., Han, B., Li, S., Ma, D., Chen, H., Ao, Y., 2018. Simulated cold bias being improved by using MODIS time-varying albedo in the Tibetan plateau in WRF model. Environ. Res. Lett. 13, 44028.

Mlawer, E.J., Taubman, S.J., Brown, P.D., Iacono, M.J., Clough, S.A., 1997. Radiative transfer for inhomogeneous atmospheres: RRTM, a validated correlated-k model for the longwave. J. Geophys. Res. Atmos. 102, 16663–16682.

Pham, H.T., Kim, S., Marshall, L., Johnson, F., 2019. Using 3D robust smoothing to fill land surface temperature gaps at the continental scale. Int. J. Appl. Earth Obs. Geoinf. 82, 101879.

Quan, J., Zhan, W., Ma, T., Du, Y., Guo, Z., Qin, B., 2018. An integrated model for generating hourly Landsat-like land surface temperatures over heterogeneous landscapes. Remote Sens. Environ. 206, 403–423.

Schädlich, S., Göttsche, F.M., Olesen, F.-S., 2001. Influence of land surface parameters and atmosphere on METEOSAT brightness temperatures and generation of land

surface temperature maps by temporally and spatially interpolating atmospheric correction. Remote Sens. Environ. 75, 39–46.
Schicker, I., Arias, D.A., Seibert, P., 2016. Influences of updated land-use datasets on WRF simulations for two Austrian regions. Meteorog. Atmos. Phys. 128, 279–301.
Sertel, E., Robock, A., Ormeci, C., 2010. Impacts of land cover data quality on regional climate simulations. Int. J. Climatol. 30, 1942–1953.
Shiff, S., Helman, D., Lensky, I.M., 2021. Worldwide continuous gap-filled MODIS land surface temperature dataset. Sci. Data 8, 1–10.
Skamarock, W.C., Klemp, J.B., Dudhia, J., Gill, D.O., Liu, Z., Berner, J., Wang, W., Powers, J.G., Duda, M.G., Barker, D.M., 2019. A Description of the Advanced research WRF Model Version 4, 145. National Center for Atmospheric RESEARCH, Boulder, CO, USA, p. 145.
Srivastava, P.K., Islam, T., Gupta, M., Petropoulos, G., Dai, Q., 2015. WRF dynamical downscaling and bias correction schemes for NCEP estimated hydro-meteorological variables. Water Resour. Manag. 29, 2267–2284.
Tewari, M., Chen, F., Wang, W., Dudhia, J., LeMone, M.A., Mitchell, K., Ek, M., Gayno, G., Wegiel, J., Cuenca, R.H., 2004. Implementation and verification of the unified NOAH land surface model in the WRF model. In: 20th Conference on Weather Analysis and Forecasting/16th Conference on Numerical Weather PREDICTION. US Census Bureau, 2019.
United States Census Bureau, 2020, April 1. Quick facts Polk County, Iowa; United Sates population. United States Department of Commerce. https://www.census.gov/quickfacts/fact/table/polkcountyiowa,US/POP010220#POP010220.
Vahmani, P., Ban-Weiss, G.A., 2016. Impact of remotely sensed albedo and vegetation fraction on simulation of urban climate in WRF-urban canopy model: a case study of the urban heat island in Los Angeles. J. Geophys. Res. Atmos. 121, 1511–1531.
Vahmani, P., Hogue, T.S., 2014. High-resolution land surface modeling utilizing remote sensing parameters and the Noah UCM: a case study in the Los Angeles Basin. Hydrol. Earth Syst. Sci. 18, 4791–4806.
Wan, Z., 2014. New refinements and validation of the collection-6 MODIS land-surface temperature/emissivity product. Remote Sens. Environ. 140, 36–45.
Wan, Z., Dozier, J., 1996. A generalized split-window algorithm for retrieving land-surface temperature from space. IEEE Trans. Geosci. Remote Sens. 34, 892–905.
Wang, Q., Huang, R., 2024. RES-STF: Spatio-temporal fusion of VIIRS and Landsat land surface temperature based on Restormer. J. Remote Sens. 4, 0208 https://doi.org/10.34133/remotesensing.0208.
Wang, K., Liang, S., 2009. Evaluation of ASTER and MODIS land surface temperature and emissivity products using long-term surface longwave radiation observations at SURFRAD sites. Remote Sens. Environ. 113, 1556–1565.
Weng, Q., Fu, P., 2014. Modeling diurnal land temperature cycles over Los Angeles using downscaled GOES imagery. ISPRS J. Photogramm. Remote Sens. 97, 78–88.
Wu, P., Shen, H., Ai, T., Liu, Y., 2013. Land-surface temperature retrieval at high spatial and temporal resolutions based on multi-sensor fusion. Int. J. Digit. Earth 6, 113–133.
Wu, P., Shen, H., Zhang, L., Göttsche, F.-M., 2015. Integrated fusion of multi-scale polar-orbiting and geostationary satellite observations for the mapping of high spatial and temporal resolution land surface temperature. Remote Sens. Environ. 156, 169–181.
Xia, G., Cervarich, M.C., Roy, S.B., Zhou, L., Minder, J.R., Jimenez, P.A., Freedman, J.M., 2017. Simulating impacts of real-world wind farms on land surface temperature using the WRF model: validation with observations. Mon. Weather Rev. 145, 4813–4836.
Yu, Y., Renzullo, L.J., McVicar, T.R., Malone, B.P., Tian, S., 2023. Generating daily 100 m resolution land surface temperature estimates continentally using an unbiased spatiotemporal fusion approach. Remote Sens. Environ. 297, 113784.
Zakšek, K., Oštir, K., 2012. Downscaling land surface temperature for urban heat island diurnal cycle analysis. Remote Sens. Environ. 117, 114–124.
Zhang, X., Chen, W., Chen, Z., Yang, F., Meng, C., Gou, P., Zhang, F., Feng, J., Li, G., Wang, Z., 2022a. Construction of cloud-free MODIS-like land surface temperatures coupled with a regional weather research and forecasting (WRF) model. Atmos. Environ. 283, 119190.
Zhang, F., Zhang, X., Chen, W., Yang, B., Chen, Z., Tang, H., Wang, Z., Bi, P., Yang, L., Li, G., 2022b. Cloud-free land surface temperature reconstructions based on MODIS measurements and numerical simulations for characterizing surface urban heat islands. IEEE J. Sel. Top. Appl. Earth Obs. Remote Sens. 15, 6882–6898.
Zhang, T., Zhou, Y., Zhao, K., Zhu, Z., Chen, G., Hu, J., Wang, L., 2022c. A global dataset of daily near-surface air temperature at 1-km resolution (2003−2020). Earth Syst. Sci. Data Discuss. 2022, 1–18.
Zhang, X., Meng, C., Gou, P., Huang, Y., Ma, Y., Ma, W., Wang, Z., Hu, Z., 2024. Evaluating the reconstructed all-weather land surface temperature for urban Heat Island analysis. Remote Sens. 16, 373.
Zhang, T., Zhou, Y., Zhu, Z., Li, X., Asrar, G.R., 2022d. A global seamless 1 km resolution daily land surface temperature dataset (2003–2020). Earth Syst. Sci. Data 14, 651–664. https://doi.org/10.5194/essd-14-651-2022.
Zhao, G., Zhang, Y., Tan, J., Li, C., Ren, Y., 2020. A data fusion modeling framework for retrieval of land surface temperature from Landsat-8 and MODIS data. Sensors 20, 4337.
Zhou, Y., Li, X., Asrar, G.R., Smith, S.J., Imhoff, M., 2018. A global record of annual urban dynamics (1992–2013) from nighttime lights. Remote Sens. Environ. 219, 206–220.
Zhu, X., Duan, S.-B., Li, Z.-L., Wu, P., Wu, H., Zhao, W., Qian, Y., 2022. Reconstruction of land surface temperature under cloudy conditions from Landsat 8 data using annual temperature cycle model. Remote Sens. Environ. 281, 113261.